



*Universidade de Vigo*



*University of Chemical  
Technology and Metallurgy*

MASTER THESIS

INFLUENCE OF THE OXIDATION STATE  
OF Ce-IONS AND THEIR  
CONCENTRATION ON INHIBITION  
EFFECT OF THE AA2024 ALLOY  
CORROSION IN A MODEL CORROSIVE  
MEDIUM

HEAD OF DEPARTMENT: .....

SUPERVISOR: .....

TUTOR: .....

REFEREE: .....

AUTHOR: Javier Expósito Pernas.....

**Sofia, April 2011**

## ACKNOWLEDGEMENTS

This research project would not have been possible without the support of many people. The author wishes to express his gratitude to Dr. S. Kozhukharov, Assoc. Prof. Dr. M. Machkova, Assoc. Prof. Dr. I. Nenov, Prof. DSc. Dr. Vl. Kozhukharov, , all from UCTM- Sofia (LAMAR department), without whose knowledge and assistance this study would not have been successful.

Special thanks also to all his graduate friends, especially PhD student Emad Matter for sharing the literature and invaluable assistance. Not forgetting to his bestfriends who always been there.

The author would also like to convey thanks to the EC– ERASMUS office and from the Bulgarian NSF, contract DVU-02/102, particularly to Gustavo Pelaez for the chance to live this enriching experience

Last but not least, the author wishes to express her love and gratitude to his beloved families and to Ester for their understanding and endless love, through the duration of his studies.

Javier Expósito Pernas.

## CONTENTS:

### I. THEORETICAL PART

#### 1. Introduction

1.1. Importance of aluminium alloy AA2024 in the industry.....	4
1.2. Significance and necessity for development of advanced corrosion protective coatings for aluminum alloys.....	5
1.3. Mechanism of corrosion of AA2024 – aluminium alloy.....	6
1.4. Concepts for active and passive corrosion protection.....	10
1.5. Environmentally friendly corrosion inhibitors.....	10
1.6. Basic electrochemical terminology.....	14
1.7. Influence of the pH and stability diagrams.....	22
1.8. Linear Sweep Voltammetry.....	23
1.9. Basic principles in the Electrochemical Impedance Spectroscopy...26	
1.10. Data presentation of EIS measurements.....	29
1.11. Deviations of the spectra of the electrochemical cells from the electrotechnical electric circuits.....	33
1.12. Modeling in the EIS. Equivalent circuits.....	35
1.13. Verification of the reliability of the EIS measurements and modeling.....	37
1.14. Equipments and methods for surface observations.....	39

### II. AIMS OF STUDY

2. Propose of experimental work.....	42
--------------------------------------	----

### III. EXPERIMENTAL

#### 3. Objects of research

3.1. Description of the objects of research.....	43
--	----

3.2.Methods and equipment of measurements.....	44
3.3.Electrochemical measurements.....	45
3.4.Topographic observations.....	45
IV. RESULTS OF MEASUREMENTS	
4. Results obtained	
4.1.Equivalent circuit employed for the object of research.....	46
4.2.Results obtained by application of Modeling by equivalent electric circuits.....	47
4.3.Results obtained by polarization curves.....	49
V. DISCUSSIONS OF THE RESULTS OBTAINED	
5. Results and discussions	
5.1.EIS measurements.....	51
5.2.EIS modeling.....	54
5.3.Polarization measurements.....	55
5.4.Surface topology observations.....	61
VI. CONCLUSIONS	
6. Conclusions over the results obtained.....	65
VII. REFERENCES	
7. References.....	67

# I. THEORETICAL PART:

## 1. Introduction:

### 1.1. Importance of AA2024 aluminium alloy in the industry

It is well known that aluminium is among the basic materials, due to its specific characteristics, it is widely used as a material for automobiles, aviation, household appliances, containers and even electronic devices.

The AA2024 alloy is the object of special attention, due to its remarkable mechanical strength [1] is used in the aircraft industry for production of different metal constructions and elements. For example, this alloy is employing in the construction of the fuselages of Airbus [2].

This alloy is the most common of the high-strength aluminum alloys because of its strength and low density. It has excellent fatigue resistance, but welding is generally not recommended. Typical uses for 2024-T3 aluminum sheet are aircraft skins, cowls, aircraft structures, and also for repair and restoration. The ultimate strength is 62000 PSI with a shearing strength of 40000 PSI.

Simultaneously, this alloy possesses relatively high susceptibility to local corrosion. The main reason for this susceptibility is the presence of Cu, Mn, Mg etc, which are in the form of intermetallic aggregates with different compositions. They form centers for initiation and spreading of local corrosion [3-7].

As it is observable from table 1, that alloy contains mainly Al, Cu, Mn and Mg .

**Table 1.** Nominal composition of AA2024-T3

Element	Al	Cu	Mg	Si	Fe	Mn	Zn	Ti	Others
Content (at%)	90-93	3,8-4,9	1.2-1.8	0.5	0.5	0,3–0,9	0.25	0.15	0.15

The included elements into the basic Al-matrix form intermetallic various precipitates. Among them, the S-phase intermetallic's precipitate covers almost 3% of the geometrical surface area of AA2024 alloy, which composition is described as (Al<sub>2</sub>CuMg). The second type of intermetallics which occurs in the alloy's composition is

$A_{16}(\text{Cu}, \text{Fe}, \text{Mn})$ , constituting 12% of all the precipitates. Minor concentrations of  $\text{Al}_{20}\text{Mn}_3\text{Cu}_2$ ,  $\text{Al}_2\text{Cu}$ ,  $\text{Al}_7\text{Cu}_2\text{Fe}$ , and  $(\text{Al}, \text{Cu})_6\text{Mn}$  are present in the alloy as well. All kinds of intermetallics excepting S-phase are composed of metals nobler than aluminum, thus showing cathodic character. However, the S-phase is composed of nobler copper as well as of active magnesium [3].

### ***1.2. Significance and necessity for development of advanced corrosion protective coatings for aluminum alloys:***

For the needs of the aircraft industry the aluminum is used generally in form of alloys with improved mechanical properties, expressed generally by enhanced resistance to mechanical and weather impact.

It is well known that particularly copper as an alloying element increases the corrosion rate by forming galvanic couples. Therefore, aluminium alloys with high copper content, like AA2024, corrode more easily than those alloys which possess lower copper content. The corrosion rate depends on both of the composition and local environment influence. Therefore, it is necessary to protect aluminium alloys from localised corrosion.

Over the past few decades, the corrosion protection of light weight aluminium alloys was achieved by ecologically harmful wet chemical processes like chromating or phosphating. There are intended to substitute Cr (VI), which possesses a high toxic level by clean inhibitor systems.

In the industrial practice, the metallic substrates are pre-treated before their application. Usually an organic paint is applied in order to improve adhesion between the polymer and the metal and to provide an additional long term corrosion protection, as well. So far, the mostly used pre-treatments contain chromates as active agents. However, the chromium containing compounds are strongly cancerous and are forbidden for industrial application.

Due to the ban of the use of chromium compounds in corrosion protection, a lot of scientific effort is invested into development of new corrosion protection species. Nowadays, researches push a high scientific power to design and prepare chromate replacement coatings that have excellent barrier property, self-healing effect and easy

coating ability. It is believed that silane based sol-gel technology is a promising chromate replace method. However, unlike chromium (VI), silane based sol-gel coatings mainly act as a physical barrier rather than form chemical bond with substrate. Inhibitors are necessary to release in the coating film to slow the corrosion process through self-healing effect. Among the inhibitors, rare-earth elements are generally considered to be effective and non-toxic in sol-gel coatings. Lanthanide ions can form insoluble hydroxides which can be successfully used as cathode inhibitors. They have low toxicity level and inhalation is not considered dangerous. The toxic effects of their oxides are similar to those produced by sodium chloride and they are industrially attractive. Their relative high abundance in nature makes it reasonable to use in the development of compounds corrosion protection. Among the lanthanides Cerium is the most abundant, and can be used as corrosion inhibitor at atmospheric influence and at high temperature treatment.

### 1.3. Mechanism of corrosion of AA2024 aluminium alloy

Despite of some accompanying chemical processes (such as sedimentation and precipitation of corrosion products), the corrosion of AA2024 in contact with electrolytes possesses predominantly electrochemical nature.

In brief, four stages of corrosion could be marked in the corrosion of AA2024:

a). - Initially, the most active metals of the superficial S-phase inclusions dissolve, and it is well illustrated in Figure 1:

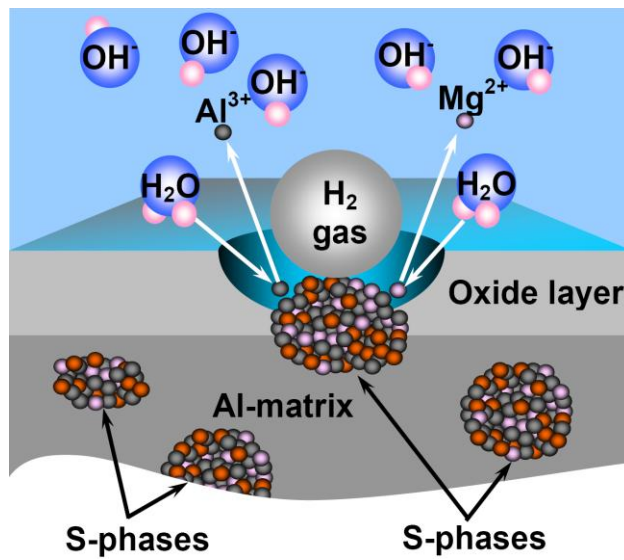
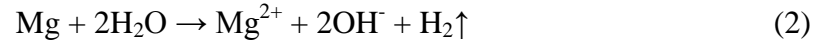
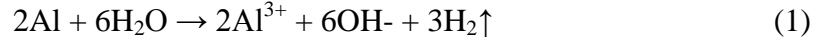


Figure 1. Initial stage of corrosion of S-phase

During this stage two kinds of chemical reactions take place, namely:

(i)- Dissolution (oxidation) of more active metals from the S-phase:



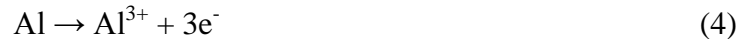
(ii)- These preliminary processes lead to changes in both of the solid S-phase, and the liquid medium (in that case solution of NaCl). The medium becomes more alkaline, while the S-phase loses Al, and Mg components, converting to copper remnants. These initial changes convert the process from purely chemical to electrochemical i.e. the second stage begins.

**b).** – The second stage is dominated by electrochemical process, where clear cathodic and anodic areas are formed. Then, the reactions on the respective areas are as follows:

*Cathodic reaction* (oxygen reduction) on copper-rich remnants which could be described by equation (3):



*Anodic reaction* (oxidation or dissolution) of more active metallic elements, as follows:



Simultaneously, the aluminium cations  $\text{Al}^{3+}$ , product of reaction 4, react with the hydroxyl anions  $\text{OH}^-$  from the liquid medium, forming sediments of  $\text{Al}(\text{OH})_3$  by passing through intermediate product  $\text{Al}(\text{OH})_4^-$ , as is shown in Figure 2:



**Figure 2.** Second (electrochemical) stage of corrosion of S-phase

Dissolution of aluminum and magnesium leads to deeper dealloying effect of the S-phase forming the porous copper remnants with “Swiss cheese”-like morphology. Consequently, the processes accelerate continuously, and the third phase begins:

c). – The third phase passes accompanied by purely chemical dissolution of the copper, followed by its precipitation in form of black coloured  $2\text{Cu(OH)}_2$  according to the following reaction:



That stage could be illustrated well in Figure 3:

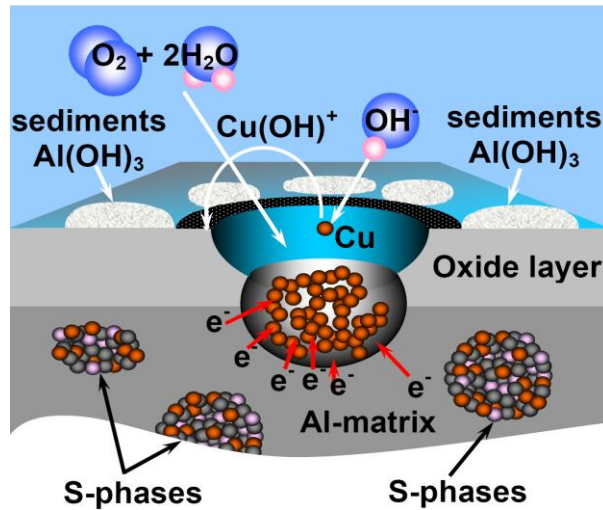


**Figure 3.** Third stage of corrosion of S-phase

**d).** – Thus, as consequence of all of the processes described above, the last phase is formation of corrosion ulcer, as it is depicted in Figure 4:

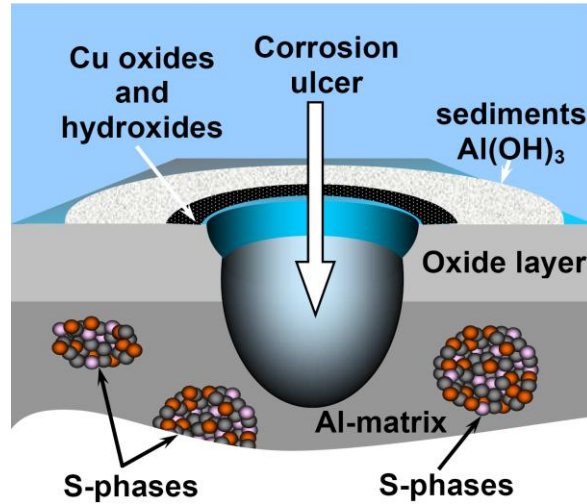


**Figure 4.** Corrosion ulcer and formation of S- phase

The Electrochemical Impedance Spectroscopy (EIS) doesn't require detailed knowledge over the chemical reactions involved in the corrosion process. When EIS is employed, it could only detect the intensity of the electrochemical reactions (3, 4 and 5), recognizing them as Charge Transfer Reactions.

Their intensity could be determined by equivalent parameter, known as charge transfer resistance  $R_{ct}$ . Its detailed decryption will be object of next sections of the present diploma work. Here should be mentioned, there is a narrow relation between the kinetics of the electrochemical reactions, and the quantity of the charge, transferred through the respective electrochemical system. This relation is described by Michael Faraday, and also will be object of discussion in the next sections.

Summarizing, we should be mentioned that the chemical and electrochemical corrosion processes on the AA2024 alloy's surface possess much more sophisticated mechanism, predetermined by the simultaneous presence of various intermetallic precipitates, as is described in ref. [8]. Comparing, the highest influence among them belongs to the S-phase, as it is mentioned in section 1.1. above. Hughes [9] report that they have found simultaneous presence of nine different intermetallic precipitates with clearly distinguishable compositions, based upon  $(Al, Cu)_x(Fe, Mn)_ySi$ . All of these inclusions are potential initiators of local corrosion, due to the simultaneous presence of

nobler and more active metals, which form specific cathodic and anodic corrosion areas, respectively.

#### **1.4. *Concepts for active and passive corrosion protection***

The passive corrosion protection of the primer coatings towards aluminium alloys relays the formation of dense superficial layers with absence of whatever defects (cracks, ruptures, deviations of the thickness etc.). In addition, the mentioned superficial protective films should possess good adhesion to the metal oxide layer, in order to perform satisfying corrosion protection. On the other hand, the protective layers should reveal remarkable durability in labour conditions. Despite of the expressed durability given protective film, it always suffers deterioration of its properties due to ageing process. The deterioration could origin either from partial hydrolysis M-O-R bonds of the composing alkoxides, or damage from external source.

The active corrosion protection should reveal after damage already represented in the structure of the protective coating. The basic approach to acquire active corrosion protective ability, is by introduction of corrosion inhibitor into the composition of the protective layer. This class of substances (corrosion inhibitors) could be described as compounds which are able to hinder or retard the corrosion processes occurring in the zone of the defects represented in the structure of the protective layer. The mechanisms of their activity in short are described below in the present text.

#### **1.5. *Environmentally friendly corrosion inhibitors***

Generally, the mechanisms of corrosion inhibition are based on formation of secondary, derivative protective film in the defects zones of the protective layer. These derivative films could be product of chemical reactions between inhibitor and compounds originated from the corrosive medium, or alternatively – between the inhibitor and whatever corrosion product. According to Yasakau et al. [3], the cerium ions derived from dissolution the respective Ce-salt react with the OH<sup>-</sup> ions, originated from the cathodic reaction of oxygen reduction as shown in equation (3). As a result, derivative barrier layer is forming composed by insoluble Ce-hydroxides, as will be described below.

The active corrosion protection should reveal after disruption of the integrity of the primer coating's structure. It means that the respective protective layer should continue to protect the metal substrate even after defect appearance. This additive protection could be realized via introduction of appropriate corrosion inhibitor.

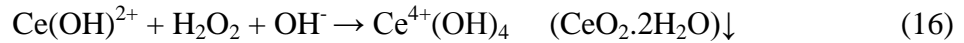
It is well known that the chromium conversion coatings (CCC) were widely used in the industry during decades [10]. However, the use of chromium was forbidden for applications in the European electronic industry by the "Restriction of Hazardous substances" (RoHS) directive and its application was for corrosion protection in the automotive industry has been banned since 2007 by the "End of life vehicles" (ELV) directive [11], as well. These actual directives have stimulated worldwide research activity over invention of new efficient and also environmentally-friendly substitutions of chromium compounds and other heavy metals. [12, 13, 14]. In this context, the compounds of the lanthanide elements have found to be the most promising among the potential substitutions of the chromium [3, 15]. Voevodin and co-authors [16] have investigated the corrosion protection abilities of epoxy-ZrO<sub>2</sub> hybrid coatings with included Ce(NO<sub>3</sub>)<sub>3</sub>, NaVO<sub>3</sub> and NaMoO<sub>4</sub> inhibitors. As a result, they have established that Ce(NO<sub>3</sub>)<sub>3</sub> reveals the highest inhibitive activity. In addition, according to Hamdy and Beccaria [17] cerium compounds reveal the best inhibitive efficient among the lanthanides. Further, they established that the inhibition rate of CeCl<sub>3</sub> is similar to this of the chromates. The inhibition mechanism of the Ce-compounds is based on deposition of insoluble Ce(OH)<sub>3</sub> and Ce(OH)<sub>4</sub> which lead to formation of a derivative barrier layer, as is described in detail by Yasakau [3]. This mechanism is based on the following reactions:



Having into account that cerium hydroxide deposits are form only over the cathodic zones, the cerium salts are generally recognized as cathodic inhibitors. The reason for this phenomenon is that the hydroxide ions are product of the cathodic reaction of oxygen reduction. Consequently, abundance of hydroxide ions occurs over the cathodic zones. Alternative mechanism is represented by Aldykiewicz and Davenport [18]. According to these authors, the conversion of the Ce-compounds to insoluble cerium hydroxides passes through oxidation of  $Ce^{3+}$  to  $Ce^{4+}$  provoked by  $H_2O_2$  which is intermediate product of the cathodic reaction of oxygen reduction, which could be represented as follows:



On the other hand, the peroxide converts the cerium ions to  $CeO_2$  according to the following reactions where one of them should be predominant in dependence of pH value of the medium [18-20].



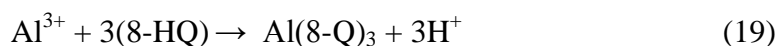
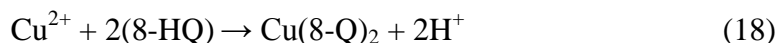
This mechanism is accepted also by other authors [21], who have investigated the corrosion behaviour of AA2024-T3, coated by metrakryloxypropylmethoxysilane with addition of cerium nitrate as inhibitor.

Other authors [19] propose an additive beneficial effect of catalysis of polymerization reaction during synthesis of the hybrid coatings, initiated by  $Ce^{4+}$  ions, due to their oxidation activity. The authors have used cerium-ammonium nitrate suggesting that this complex salt improve the barrier ability of the corresponding hybrid coatings, consisted on biss-(triethoxysilil) ethane. The improving effect could be consequence of formation of additive organic-complex bridges, as it is investigated by different authors [19, 22-24].

However, other authors have reported for deterioration effect over the barrier ability of hybrid primer coatings caused by the addition of  $Ce(NO_3)_3$  into their

compositions. Similar effect was also observed after involvement of various inorganic inhibitors into a hybrid material composed by  $(C_3H_7O)_4Zr$  and GPTS [16]. The authors performed comparative investigations over several inhibitors, such as:  $Na_2Cr_2O_7$ ,  $Ce(NO_3)_3$ ,  $Na_2MoO_4$  and  $NaVO_3$ . As conclusion they have established that all of the investigated inhibitors involved into the corresponding sol-gel systems deteriorate the barrier ability of the respective hybrid primer coatings. The highest rate of deterioration was established for  $Na_2MoO_4$  and  $NaVO_3$ . The authors explain deterioration effect having in account that when these salts are added into the composition of the hybrid matrix primer coating, they crystallize. After contact of the respective crystals with NaCl solution, they dissolve leaving cavities on their positions. The obtained cavities facilitate the access of the species from the corrosive medium towards the metal surface.

Alternatively, some organic substances also could be applied as corrosion inhibitors, and for example, 8-hydroxyquinoline (8-HQ) is an effective compound. Different authors convince that this compound could be successfully applied as cathodic inhibitors [25-28]. The inhibition effect, in that case, is based on the formation of weakly soluble complexes with the copper and the aluminium in neutral medium, according to reactions (18) and (19):



Another authors have performed large comparative research over the impact of a different lanthanide salts (  $La(NO_3)_3$ ,  $Y(NO_3)_3$ ,  $Ce(NO_3)_3$  ) as well as some organic substances (represented in Figure 5) over the corrosion inhibition.

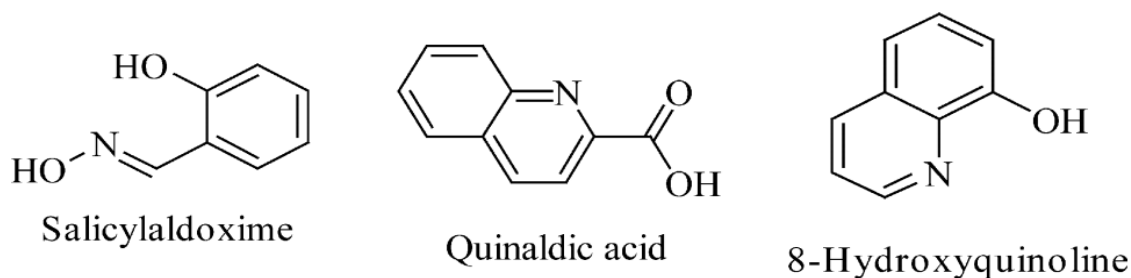


**Figure 5.** Examples for selected organic inhibitors [28]

Other examples for corrosion inhibition efficiency via organics substances have been object of study, as for example benzotriazole [29, 30] and Thoulyl triazole [30]. It was established that potential exists for application of these substances as corrosion inhibitors as well. In the present case, the principals of their corrosion inhibitive effect is based on the formation of insoluble complex which form sediments on the metal's surface and by that manner they hinder the access of the corrosion species towards to the metal surface.

### **1.6. Basic electrochemical terminology**

As it was described in the section 1.3 the superficial corrosion has predominantly electrochemical character. Consequently, the application of electrochemical analytical methods is the most appropriated approach for determination of corrosion processes, as well as its description. Furthermore, this group of methods enables to perform both of quantitative assessment, and qualitative evaluation. The former, corresponds to determination of the corrosion rate, or by other words – the kinetics of the corrosion process. The latter, is related to definition of the nature of the electrochemical reactions, which compose the corrosion process.

The topography of the corrosion surface process could be easily determined by additive microscopic observations. Here, should be mentioned that the corrosion process could pass in form of uniform or localized (pitting, intergannular, filliform, etc. [31] surface corrosion defects).

In short, the investigations over the corrosion processes involve: the nature electrochemical chemical reactions, their kinetics, as well as topography study of the corrosion surface. The corrosion often passes by simultaneous presence of different processes. Their nature and rate completely depend on three basic factors, as follows:

- 1- The chemical composition of the metal alloy and the properties of the composing metals.
- 2- The environment influence and the nature of surrounding chemical interaction, especially its pH value.
- 3- The parameters of the environment – temperature, pressure, presence of mechanical impact, exposed area of the metal, etc.

The last one depends on the shape and design of the metallic detail, presence or absence of protective coatings and their properties, superficial roughness, etc.

Besides the electrochemical nature of the corrosion processes, as described by Petrucci, as “undesirable voltaic cells” [32], they have generally heterogeneous character. The corroding alloy’s surface is always in solid state, and the surrounding environment is usually in liquid phase. Sometimes the corrosion could pass between solid alloy and gaseous aggressive environment (for example: the walls and tubes of water evaporators in thermal electric stations, chemical reactors, etc.).

Thus, the electrochemical reactions, composing the corrosion (cathodic - reduction, and anodic - oxidation), pass by transfer of electrons, and always through interface region. The heterogeneous chemical and electrochemical reactions are always composed by:

- 1- Adsorption of species on the solid surface.
- 2- Chemical/electrochemical process interaction.
- 3- Desorption of the obtained products.
- 4- Diffusion of the products with the species in the medium [33].

The rate of whatever heterogeneous electrochemical reaction ( $v$ ) could be defined by the quantity of reagent e.g. metal or corrosive species (in mols), treatment for converted for given unit of time (s) and through given unit of surface ( $m^2$ ), according to equation (20):

$$v = 1/A \frac{dm}{dt} \quad (\text{mol/cm}^2 \text{ s}) \quad , \quad (20)$$

where:  $dm/dt$  is the quantity of given substance underwent chemical conversion for a period of time, through any defined surface.

In order to have in account the participation of electrons, the equation 20 should be connected to the Faraday’s law: “For the electrochemical conversion of one equivalent weight of whatever substance, it is necessary the same quantity of electrons, equal to 1 Farad”, or:

$$i = nFv \quad (\text{A/cm}^2) \quad , \quad (21)$$

where:  $n$  is the number of transferred (exchanged) electrons, and  $i$  is the current density  $A/cm^2$ . Alternatively, the same dependence could be described as follows [34]:

$$I_{corr}t = \frac{nFw}{M} \quad (\text{Coulomb}) , \quad (22)$$

where:  $I_{corr}$  is the corrosion current at steady state. In this context, it is important to describe in short some corrosion electrochemical parameters, as follows:

- **Corrosion currents:** the  $I_{corr}$  of a given corroding alloy is related to the electric charges (electrons) transferred from the anodic zones to the cathodic zones through the bulk of the corroding alloy. It is technically impossible to measure directly  $I_{corr}$ , because the cathodic and anodic zones are connected “short connection” in the alloy. On the other hand,  $I_{corr}$  entirely predetermines the corrosion rate (measured often as mm/year for uniform corrosion). Since the electrons which leave the anodic areas, are the same, which enter into the cathodic zones, the entire anodic current  $I_a$  is equal to the entire cathodic current  $I_c$ .

In addition, there may be more than one cathodic reaction (i.e., more than one “ $I_c$ ”) and more than one anodic reaction [34].

$$I_{corr} = \sum I_a = -\sum I_c \quad (23)$$

Consequently:  $(\sum I_a - \sum I_c) = 0$ , or the system, composed by corroding metal and corrosive environment is in steady state.

- **Corrosion current density,  $i_{corr}$ :** The fact that the anodic and cathodic corrosion currents are equal doesn't mean that the corresponding current densities are also equal. Because the areas of anodic regions ( $A_a$ ), are generally different from the areas of cathodic regions ( $A_c$ ), current densities are generally not equal, and according to ref. [34] can be expressed as follows :

$$I_a = i_a/A_a \neq i_c/A_c = I_c \quad (24)$$

- **Corrosion potential**  $E_{\text{corr}}$ : It is clear that the corrosion currents, as the currents in the electrotechnique are directly related to potential's difference between two points of a given electric chain. The potential difference, where the latter is the electromotive power which makes the electrons to move in given direction (in the case of corrosion – from the anodic areas to the cathodic).

The origin of  $E_{\text{corr}}$  is directly related to the difference of the energies necessary to apply to the atomic structures of different metals to render valent electrons (to convert to ions). This energy is described in thermodynamics as variation of the Gibb's free energy at standard conditions  $\Delta G^0$ . Thus, it is necessary to apply some energy to given metal atoms, for rendering of electron. This energy is necessary for the atomic structures to overcome a potential barrier for rendering of electrons (i.e: ionization). The potential barriers are different for the different elements of the Periodic system. They are related to the properties of the elements, such as electronegativity and the affinity to the electrons. Consequently, the nobler metals (Pt, Au, Ag) possess higher affinity to the electrons, coupled with lower electronegativity than the more active (Li, Na, K, Mg ect.).

Namely, because of this difference, the corrosion process has a spontaneous character. Other reason for the spontaneity of the corrosion is that always the systems in the nature endeavor to convert from higher level of ordering, to lower order, which is related to their entropy  $\Delta S$ .

Fortunately, the corrosion potential could be directly measured against a standard electrode. Its potential is conditionally accepted as zero. The potential of whatever electrode, measured against a standard electrode is known as electrode's potential.

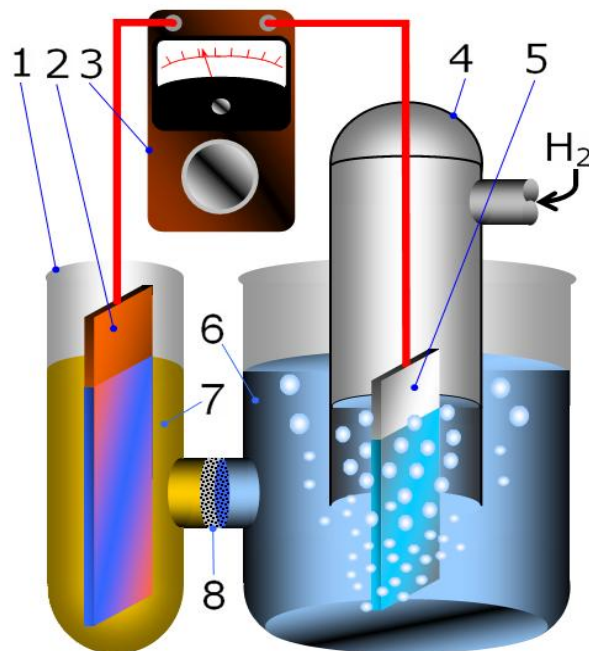


**Figure 6.** Schematic presentation of measurement of electrode potential by Standard Hydrogen Electrode (SHE)

- 1- glass vessel; 2- measured electrode; 3- milivolt meter (galvanometer); 4- gas bell; 5- platinum plate; 6- and 7- electrolytes; 8- semipermeable membrane

Figure 6 shows a schematic view of a system for electrode potential measurement unit. The SHE electrode is in state of equilibrium between the concentration of  $H^+$  ions and the  $H_2$  gas dissolved in the medium. Its construction in detail is described in the literature [35]. The Standard Hydrogen Electrode (SHE) serves for determination of the potential's difference between the metal and its ions in the surrounding electrolyte in conditions of equilibrium. This equilibrium is represented between the reduced and the oxydized forms of the metal. The latter is represented in form of dissolved ions ( $Me^{n+}$ ) in the liquid medium, while the reduced form is in form of solid metal ( $Me^0_{solid}$ ).



The standard electrode potentials are determined for a large number of Red/Ox couples, and they could be found in ref. [35 - 37]. Selected example for table of standard potentials is represented in Table 2:

**Table 2:** Standard electrode's potentials for various Red/Ox couples [36]

Red / Ox	Electrode reaction	$E^{\theta}$ Volts/SHE
Li Li <sup>+</sup>	Li <sup>+</sup> + e <sup>-</sup> ⇌ Li	-3,040
Rb Rb <sup>+</sup>	Rb <sup>+</sup> + e <sup>-</sup> ⇌ Rb	-2,924
K K <sup>+</sup>	K <sup>+</sup> + e <sup>-</sup> ⇌ K	-2,924
Cs Cs <sup>+</sup>	Cs <sup>+</sup> + e <sup>-</sup> ⇌ Cs	-2,923
Ca Ca <sup>2+</sup>	Ca <sup>2+</sup> + 2e <sup>-</sup> ⇌ Ca	-2,76
Na Na <sup>+</sup>	Na <sup>+</sup> + e <sup>-</sup> ⇌ Na	-2,713
Mg Mg <sup>2+</sup>	Mg <sup>2+</sup> + 2e <sup>-</sup> ⇌ Mg	-2,375
Al Al <sup>3+</sup>	Al <sup>3+</sup> + 3e <sup>-</sup> ⇌ Al	-1,706
Zn Zn <sup>2+</sup>	Zn <sup>2+</sup> + 2e <sup>-</sup> ⇌ Zn	-0,7628
Pt Cr <sup>2+</sup> , Cr <sup>3+</sup>	Cr <sup>3+</sup> + e <sup>-</sup> ⇌ Cr <sup>2+</sup>	-0,41
Fe Fe <sup>2+</sup>	Fe <sup>2+</sup> + 2e <sup>-</sup> ⇌ Fe	-0,409
Cd Cd <sup>2+</sup>	Cd <sup>2+</sup> + 2e <sup>-</sup> ⇌ Cd	-0,4026
Ni Ni <sup>2+</sup>	Ni <sup>2+</sup> + 2e <sup>-</sup> ⇌ Ni	-0,23
Pb Pb <sup>2+</sup>	Pb <sup>2+</sup> + 2e <sup>-</sup> ⇌ Pb	-0,1263
Pt H <sub>2</sub> , H <sub>aq</sub> <sup>+</sup>	2H <sup>+</sup> + 2e <sup>-</sup> ⇌ H <sub>2</sub>	0,0000
Pt Cu <sup>2+</sup> , Cu <sup>+</sup>	Cu <sup>2+</sup> + e <sup>-</sup> ⇌ Cu <sup>+</sup>	+0,167
Cu <sup>2+</sup>  Cu	Cu <sup>2+</sup> + 2e <sup>-</sup> ⇌ Cu	+0,3402
Pt [Fe(CN) <sub>6</sub> ] <sup>3-</sup> , [Fe(CN) <sub>6</sub> ] <sup>4-</sup>	[Fe(CN) <sub>6</sub> ] <sup>3-</sup> + e <sup>-</sup> ⇌ [Fe(CN) <sub>6</sub> ] <sup>4-</sup>	+0,356
Pt [W(CN) <sub>8</sub> ] <sup>3-</sup> , [W(CN) <sub>8</sub> ] <sup>4-</sup>	[W(CN) <sub>8</sub> ] <sup>3-</sup> + e <sup>-</sup> ⇌ [W(CN) <sub>8</sub> ] <sup>4-</sup>	+0,457
Pt [Mo(CN) <sub>8</sub> ] <sup>3-</sup> , [Mo(CN) <sub>8</sub> ] <sup>4-</sup>	[Mo(CN) <sub>8</sub> ] <sup>3-</sup> + e <sup>-</sup> ⇌ [Mo(CN) <sub>8</sub> ] <sup>4-</sup>	+0,725
Ag Ag <sup>+</sup>	Ag <sup>+</sup> + e <sup>-</sup> ⇌ Ag	+0,7996
2Hg Hg <sub>2</sub> <sup>2+</sup>	Hg <sub>2</sub> <sup>2+</sup> + 2e <sup>-</sup> ⇌ 2Hg	+0,7961
Pt Cr <sub>2</sub> O <sub>7</sub> <sup>2-</sup> , Cr <sup>3+</sup> , H <sup>+</sup>	Cr <sub>2</sub> O <sub>7</sub> <sup>2-</sup> + 14H <sup>+</sup> + 6e <sup>-</sup> ⇌ 2Cr <sup>3+</sup> + 7H <sub>2</sub> O	+1,36
Pt O <sub>2</sub> , H <sub>2</sub> O, H <sup>+</sup>	1/2O <sub>2</sub> + 2H <sup>+</sup> + 2e <sup>-</sup> ⇌ H <sub>2</sub> O	+1,229
Au <sup>+</sup>  Au	Au <sup>+</sup> + e <sup>-</sup> ⇌ Au	+1,42
Pt MnO <sub>4</sub> <sup>-</sup> , Mn <sup>2+</sup> , H <sup>+</sup>	MnO <sub>4</sub> <sup>-</sup> + 8H <sup>+</sup> + 5e <sup>-</sup> ⇌ Mn <sup>2+</sup> + 4H <sub>2</sub> O	+1,491
Pt H <sub>4</sub> XeO <sub>6</sub> , XeO <sub>3</sub>	H <sub>4</sub> XeO <sub>6</sub> + 2H <sup>+</sup> + 2e <sup>-</sup> ⇌ XeO <sub>3</sub> + 3H <sub>2</sub> O	+2,42
Pt F <sub>2</sub> , F <sup>-</sup>	F <sub>2</sub> + 2e <sup>-</sup> ⇌ 2F <sup>-</sup>	+2,866

In the practice, other standard electrodes are applied for determination of the electrode's potentials.

- **Polarization and polarization resistance:** This phenomenon appears when a potential from external source is applied over the electrode (by another – counter electrode). Then, the electrode suffers polarization. It means that is out of its steady state, and the electrochemical reactions (see equations 25, 26) are not anymore in equilibrium. When the electrode is already polarized, a measurable current appears.

The expression relating the overpotential,  $\eta$ , to the net current,  $i$ , is the Butler-Volmer equation [34]:

$$i = i_o \left\{ \exp\left(\beta \frac{nF}{RT} \eta\right) - \exp\left(-[1-\beta] \frac{nF}{RT} \eta\right) \right\} , \quad (27)$$

where:

$R$  = gas constant;

$T$  = absolute temperature;

$n$  = no. charges transferred ( $\equiv$  valency);

$F$  = Faraday constant (96,500 coul/mol);

$\beta$  = “symmetry coefficient” ( $\diamond$  0.5);

$i_o$  = exchange current density (a constant for the system).

The first exp. term in “( )” in B-V describes the forward (metal dissolution, anodic) reaction; the second exp. term in “( )” describes the backward (metal deposition, cathodic) reaction.

The graphical presentations of the polarization of given electrode survey information for the current measured, when a potential from external source is applied. They are also known as polarization curves. When the applied overpotentials  $\eta$  are more positive than  $E_{\text{corr}}$ , or  $E_{\text{Red/Ox}}$  than the obtained curves are anodic. If  $\eta$  is more negative, than the respective curve is cathodic. Figure 7, shows typical polarization curves:

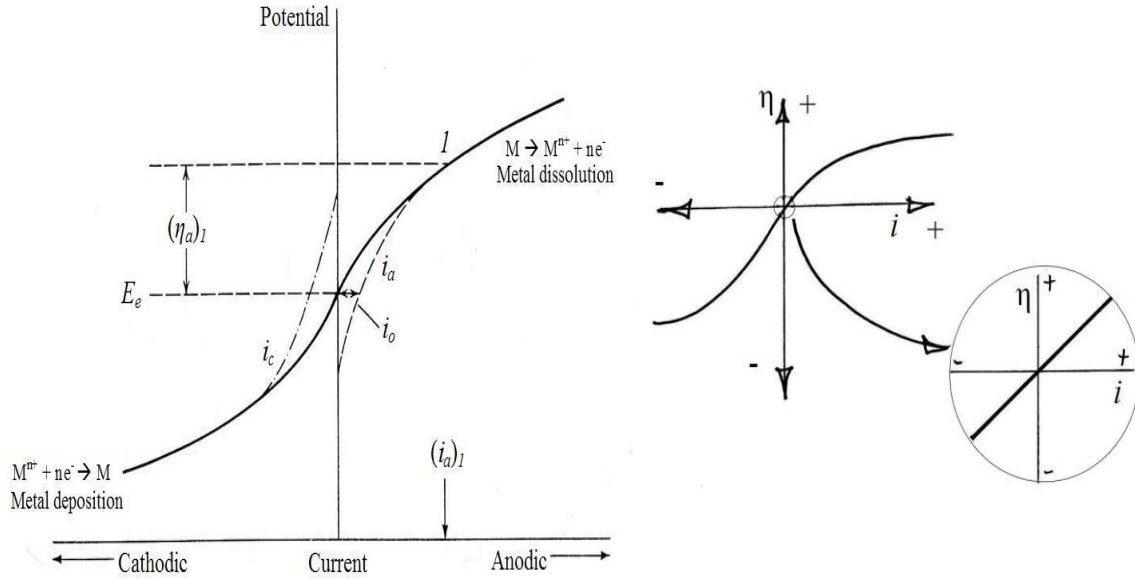


**Figure 7.** Example for polarization curve [34]

Here should be mentioned that if the overpotentials applied are enough low, the dependence between the measurable current flow, and the applied potential possesses linear form.

- **Polarization resistance:** Following Ohm's law, it could be expected that there is a relation between the measurable current, and the applied overpotential  $\eta$ .

Every kind of change of the measured current ( $\Delta I$ ) between the referent and the working electrode, caused by the change of the voltage of the input signal, ( $\Delta U$ ) between the counter electrode and the working electrode is known as "polarization". The corresponding coefficient of the mentioned relationship is known as "Polarization resistance" ( $R_p$ ).

$$R_p = \frac{\Delta U}{\Delta I} \quad (\Omega) \quad (28)$$

### 1.7. *Influence of the pH and stability diagrams*

It is well known that the pH has remarkable influence over almost all the processes in chemistry. Its value could predetermine which kind of chemical process could occur in a given system. Especially, in corrosion processes, pH predetermines which kind of cathodic processes could begin. At acidic media, the pH predestines which process (oxygen reduction or hydrogen evolution) will be the cathodic reaction. Particularly in electrochemistry, the diagrams of Pourbaix are indispensable, and they predetermine which kind of chemical compound and which electrochemical reaction should occur in a given system, taking in account the pH value and the potential. In the case of inhibition by whatever Cerium compound, the pH value predetermines which deposits of Cerium insoluble substances will occur. Consequently, in the present study the pH will predetermine the Inhibition Efficiency (IE) of given Cerium compounds used.

Two general variables, pH (chemical) and potential (electrochemical), have been identified as important to the deposition of the conversion coatings. Pourbaix diagrams (E-pH) have been used as a means to theoretically identify or indicate the conditions under which passive films are possible to form. This method has been described for chromating, and a similar approach was used to better define the cerium oxide deposition process. As an example for Ce- relations, an original Pourbaix diagram is shown in Figure 8. This diagram did not correlate well with experimental results of deposition and precipitation tests, so the Pourbaix diagram was re-examined using more recent thermodynamic data.

The revised diagram that was proposed is shown also in figure 8 (right site), and some significant changes are observed. The pH required for precipitation to cerium oxide from  $\text{Ce}^{4+}$  ions is in the range of 4.5, the region of stability of  $\text{CeO}_2$  is greater, and the possibility of the  $\text{Ce}^{3+}$  to  $\text{CeO}_2$  reaction can occur over a wider range of pH and E operating conditions.

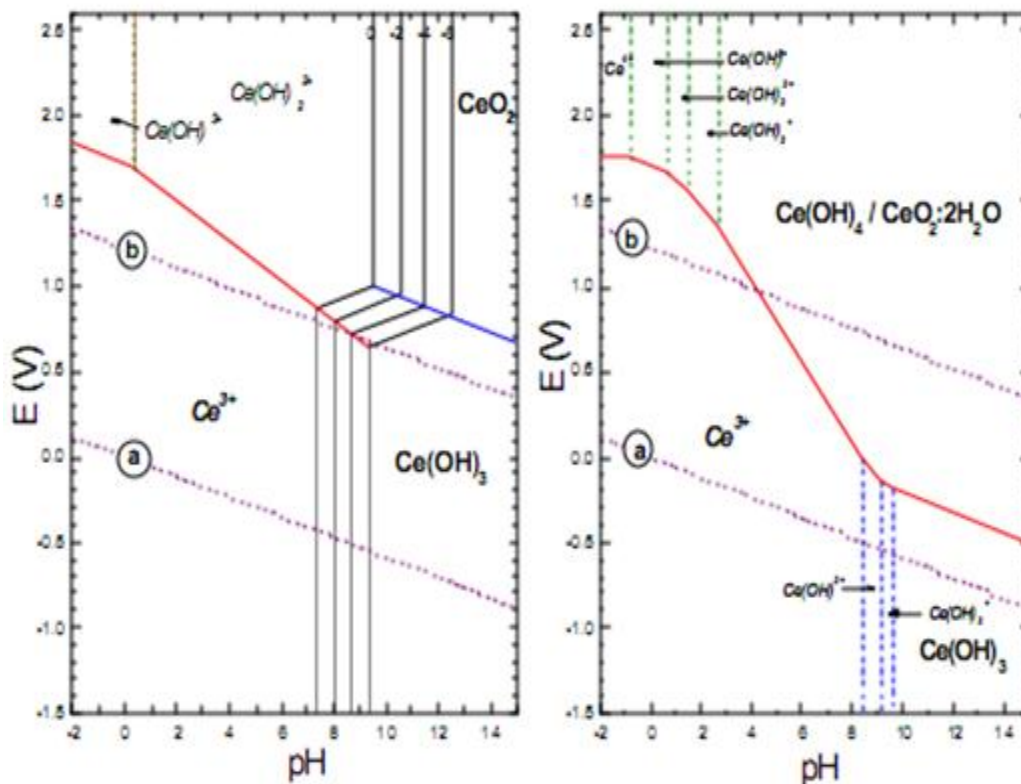


**Figure 8.** The original E-pH diagram (on the left side) and the revised E-pH diagram (on the right side) [38]

### 1.8. Linear Sweep Voltammetry

This electrochemical method is based on the measurements of the responses of an electrochemical system (cell) object of study. In this case, the measuring system measures the signals, obtained by the reference electrode. The generator produces signals with gradient variation of the voltage.

Simultaneously, the measuring system measures the current, obtained by the reference electrode. Initially, the equipment measures the open circuit potential (OCP) between the working and reference electrode. Afterwards, it inputs signal with gradual change of the voltage, between the working and the counter electrode. The initial and the final values, as well as the rate voltage increase are previously predetermined. Figure 9 presents typical plot obtained by Linear Voltammetry:

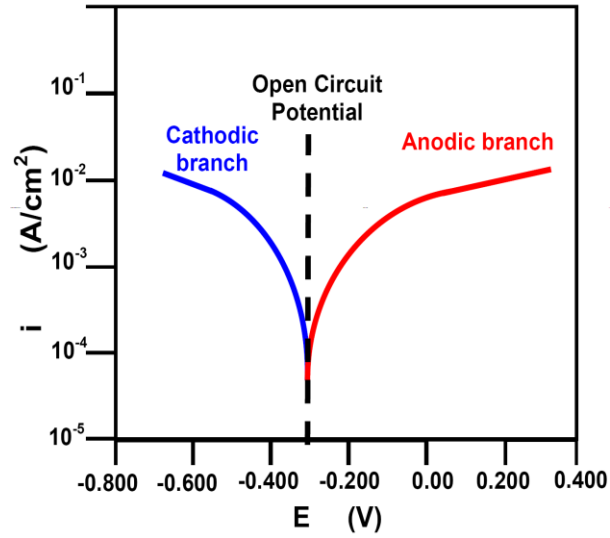


**Figure 9.** Typical plot obtained by Linear Voltammetry.

The superficial chemical composition of the samples object of investigation, suffers permanent changes due to the presence of corrosion processes. It is observable by comparison of measurement after different periods of time. By that manner, the evolution of the corrosion process within the time could be defined. Figure 10 presents the shifting of OCP, as consequence of the above mentioned permanent chemical changes.

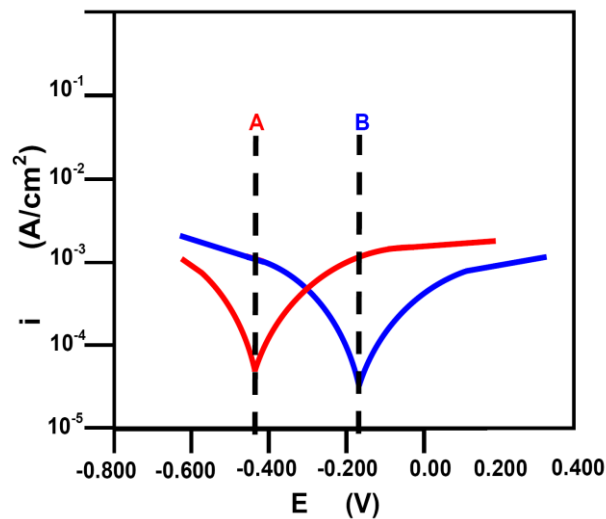


**Figure 10.** Illustration of the OCP shifting value within the time.

Just so, this shifting could be from more noble to more active state in direction from B to A, or vice versa. These changes is consequence either of the selective solubility of the different metals which compose given alloy, or re-passivation of the alloy.

Changes of the anodic and cathodic currents could be also observable. Usually, they are in direction from lower (position B) to higher (position A) values, with the time as it is well demonstrated in Figure 11. Changes in the opposite direction (from A to B) are possible as well.

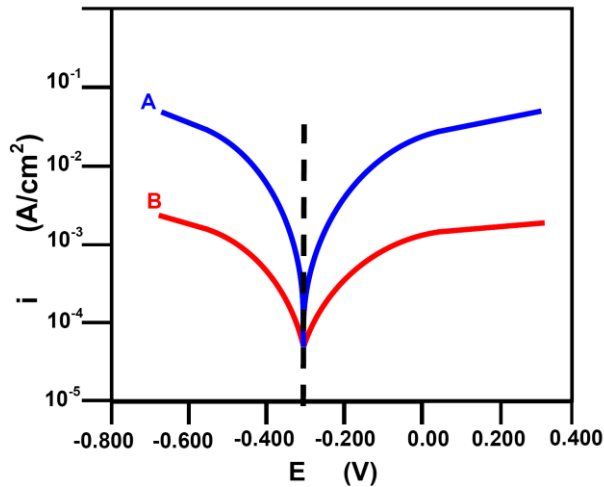


**Figure 11.** Example of typical plot obtained by Linear Voltammetry

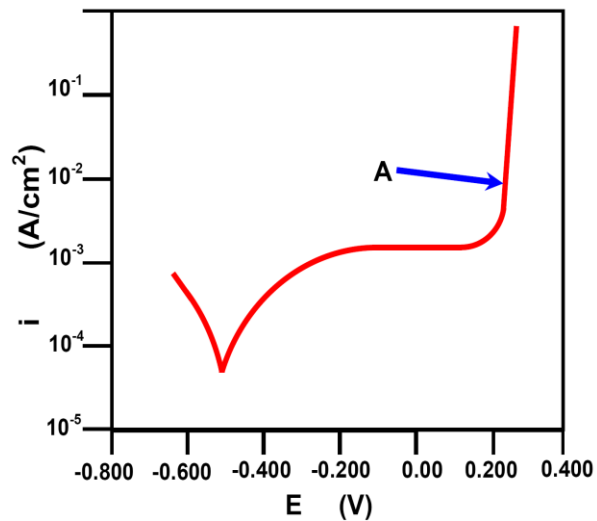


**Figure 12.** Plot obtained by Linear Voltammetry with additive declivity.

The form of the curves has also its importance. The appearance of additive deconvolvement (signed by letter A in figure 12) in the case of the aluminum alloy is clear evidence that pitting localized corrosion process occurs.

### 1.9. *Basic principles in the Electrochemical Impedance Spectroscopy*

The electrochemical Impedance Spectroscopy (EIS) is an analytical technique based on acquiring of response of all kinds of active (R) and reactive resistances (C; L) from a given electrochemical cell, at input of electric signals with different frequencies to it.

The acquiring of an impedance spectrum is based on interaction between the impedance spectrometer and the electrochemical cell. The electrochemical cells could possess different constructions and design, according the features of the objects of measurements. Hence, the cells could be with two, three or four electrode's constructions. For the needs of the corrosion test, the three-electrode cells have found the widest use. Figure 13 shows a schematic connections and control between the impedance spectrometer and an electrochemical cell .

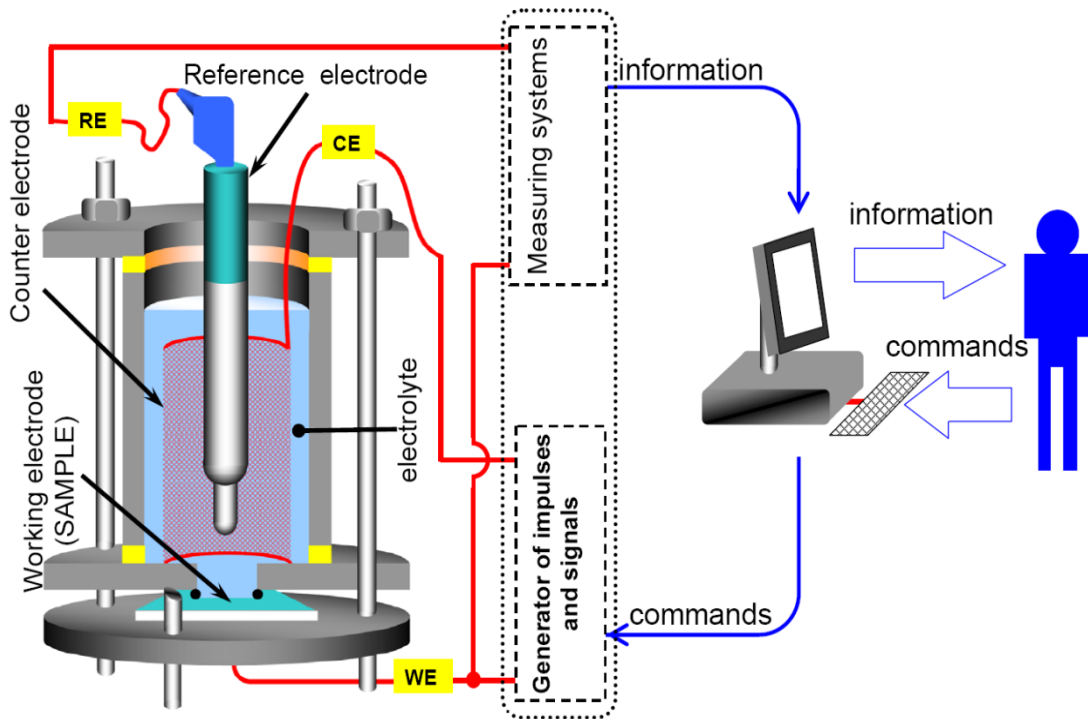


**Figure 13.** Schematic illustration of the connections and the control between three-electrode cell and impedance spectrometer.

- *Impedance spectrometer* is electronic analytical device, which generates AC excitation signals with different frequencies and transmit them by the counter electrode (CE), and measures the “answers” of the cell by the reference electrode (RE). Together with the working electrode (WE), all of the electrodes are immersed in an electrolyte. In the case of corrosion tests, the electrolyte serves simultaneously as corrosive medium, and conductive medium for transmission of charges among the electrodes.

- *Electrochemical cell* is the device of housing of the samples (objects of measurements), together with the electrolyte and electrodes. Here, should be mentioned that in whatever electrochemical cell, (galvanic or electrolytic) there are interphases between the electrodes and the electrolyte [35]. All electrochemical reactions occur on the surface of these interphase regions. These reactions could be considered of charge transfer reactions between the corresponding electrodes, and species from the liquid electrolyte. In general, the electrochemical reactions could be described as oxidation or reduction of various substances, which are always accompanied by transfer of electrons. As was mentioned above, these reactions pass on the interphases between the electrodes (solid) and the electrolyte (usually liquid), and consequently, they possess heterogeneous nature. These reactions are also known as “electrode reactions” [36]. Typical example for electrode reactions is the corrosion of alloys in aqueous solutions of salts. Particular example for corrosion of alloys in aqueous medium is the corrosion of AA2024 alloy in water solution of NaCl. In section 1.3. of present work this process was described as consisted on electrochemical local dealloying process, composed by two electrochemical reactions:

(i)- *Cathodic reaction* of oxygen reduction (see equation (3)), which occurs on the surface of the nobler (Cu) inclusions.

(ii)- *Anodic reaction* of oxidation of more active components of the alloy, leading to their dissolving (see equations (4) and (5)).

Both of reactions are accompanied by electric currents in the bulk of the alloy. These currents are known as “corrosion currents”. Their values are proportional to the quantity of the oxidized or reduced substances. Here, could be mentioned that direct measurement of the corrosion currents is impossible.

The basic parts of an electrochemical cell could be described as follows:

*Electrolyte:* The electrolyte in the electrochemical cells serves for charge transport between the electrodes, in order to close the electrical circuits.

The charge transport in the liquid electrolytes passes in form of charged ions, which exchange their electrons with the electrodes (via electrode reactions) as is described above. Hence, it could be mentioned that in the electrochemical systems the processes are much more complicated. There are overlapping characteristics from the electric (electronics and electrotechnique) and electrochemical sources as charge carriers which are ions in the electrolyte. Thus, the charge transport through electrolyte is always accompanied with processes of diffusion, and depends on the chemical composition of the electrolyte, and the concentration of its ingredients, which predetermines the electrolyte resistance  $R_{el}$ .

*Electrodes:* Principally, in electrochemistry there are two kinds of electrodes – cathodes and anodes. However, for the needs of the corrosion tests, and particularly for EIS measurements, the electrodes of the cells have more complicated role.

*Working electrode (WE):* it is a part of the investigated sample, exposed to the electrolyte. Its superficial area has exactly defined geometrical surface, in order to supply reproducibility of the measurements.

*Counter electrode (CE):* It serves to transmit the input excitation signals from the spectrometer to the cell. The circuit between the spectrometer and the cell closed through CE and WE serves to provide the excitation signals to the cell. The basic requirement for CE is that it must be composed by noble material, in order to avoid undesirable additive processes of its corrosion, which will cause confusion to the measured results, as well as contamination of the electrolyte with additive corrosion products.

*Reference electrode (RE):* It serves as reference for comparison of the potentials and currents on the interface between the surface of WE and the electrolyte. Several kinds of electrodes are available for the needs of electrochemical measurements, as follows [39]:

- *Hydrogen electrode:* It could be described as Platinum piece immersed in HCl, and blowing by hydrogen gas.
- *Callomel electrode:* It is composed by metallic Hg, in contact to  $Hg_2Cl_2$  in solution of KCl, with known concentration.

- *Silver chloride electrode*: It is metal silver wire, exposed in AgCl salt, in saturated solution of KCl (3 mol per liter).

The last two kinds of reference electrodes are usually used for the needs of EIS measurements.

In addition, here should be mentioned that the design, construction, and the materials for electrochemical cells for EIS- measurements, must correspond to industrial requirements, in order to obtain convenient reproducible results, which are not influenced by undesirable interactions between the materials of the cell, and the electrolyte. The industrial standard, which describes the requirements for the electrochemical cells, used for the purpose of EIS, as well as the appropriated conditions for performance of EIS are described by ISO 16773-2: 2007 (E) Standard [40].

The standard deals to the instrumental set-up, the conditions of EIS-measurements, the data presentation for EIS, checking of the accuracy of the data, and their interpretation via modeling by equivalent circuits. The data obtained from EIS, reveal all of the active and reactive resistances of the cell, against the input signals in the respective frequency range.

#### **1.10. *Data presentation of EIS measurements:***

After performance of EIS measurement, the obtained results from the electrochemical cell are in form of impedance spectrum for given frequency range. For the needs of corrosion processes research on coated alloys, the range is usually from 100 kHz, to 0.1 Hz, distributed in several frequency points per decade (7 – 10). Hence, the impedance spectrum reveals all of the active and reactive resistances which compose the total impedance of given electrochemical cell, measured for given frequency range of excitation signals, generated by the spectrometer. The resistances could be active (such as Ohmic) – which is frequency independent and reactive (such as Capacitance or Inductance) – which values depend on the frequency of the excitation signal.

Generally two kinds of plots of a recorded impedance spectrum exist and they are as follows:

- **Nyquist plot:** It is a linear graph in complex plane of imaginary part of the impedance  $Z''$ - related to the reactive resistances (negative for capacitance and positive for inductance), versus real part  $Z'$ , which relates to the active resistance.

- **Bode plot:** It is double logarithmic graph, of the modulus of the total impedance  $[Z]$  for each frequency point, linear presentation of the phase shift ( $\phi$ ), against logarithm of the frequency ( $\log f$ ).

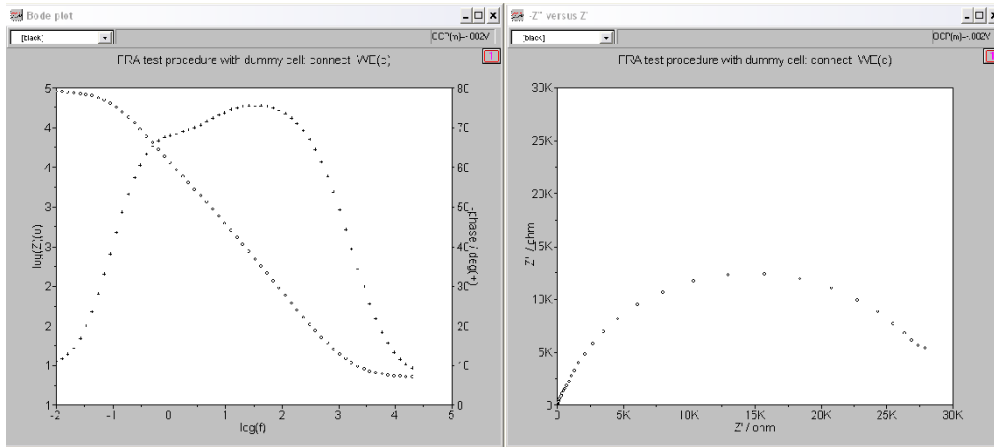


**Figure 14.** Typical Bode plot on the left and Nyquist plot on the right

The mentioned active and reactive resistances of the electrochemical cell are function of their origin in dependence of the electrolyte and the working electrode used, as follows:

- **Active resistance:** It owes its origin generally to the resistance of the electrolyte. Its resistance and conductivity, respectively depends on the chemical nature of the ions, and also their concentration, as is shown in Figure 15:

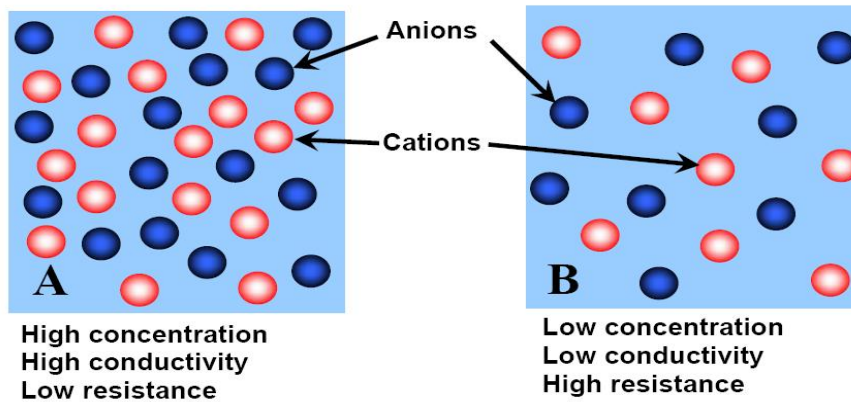


**Figure 15.** Schematic illustration of the electrolyte characteristics

As it was mentioned above, the charge carriers in the electrolyte are ions. When their concentration is too high, it is possible to detect increase of the electrolyte resistance. The reason for this phenomenon is to decrease the mobility of each ion due to formation of surrounding clouds, of attracted water dipoles around the ion, as is shown below:

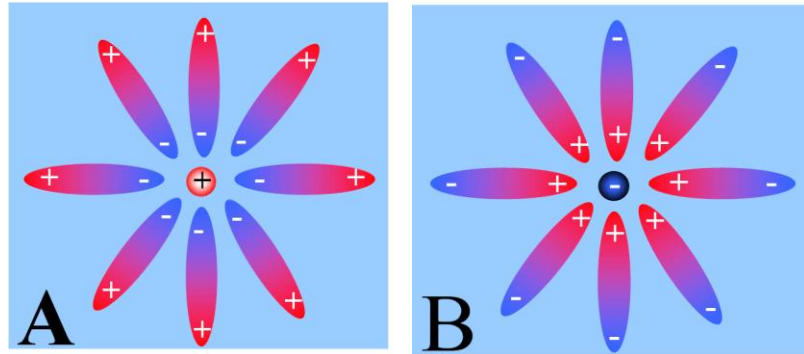


**Figure 16.** Schematic view of dipole's clouds around a cation (A), and around anion (B)

In addition, the active resistance is related to all processes involved to charge transport in the bulk of given homogeneous phase. When the object of research is corrosion of metals, always there is resistance of the charge transfer cathodic (reduction) and anodic (oxidation) partial electrochemical reactions. It is known as Charge transfer resistance ( $R_{ct}$ ) or polarization resistance ( $R_p$ ).

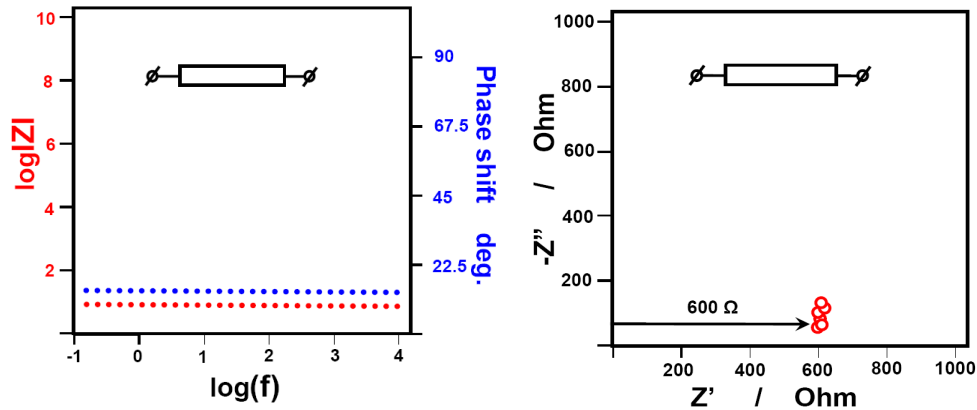


**Figure 17.** Bode and Nyquist plots characteristics of an active resistance respectively.

- **Capacitive (reactive) resistance:** As it was mentioned above, whatever electrochemical cell is composed by electrodes, immersed in electrolyte. It means that in

every electrochemical cell there are interfaces represented on the surface of the electrodes, as it is represented on the next figure:

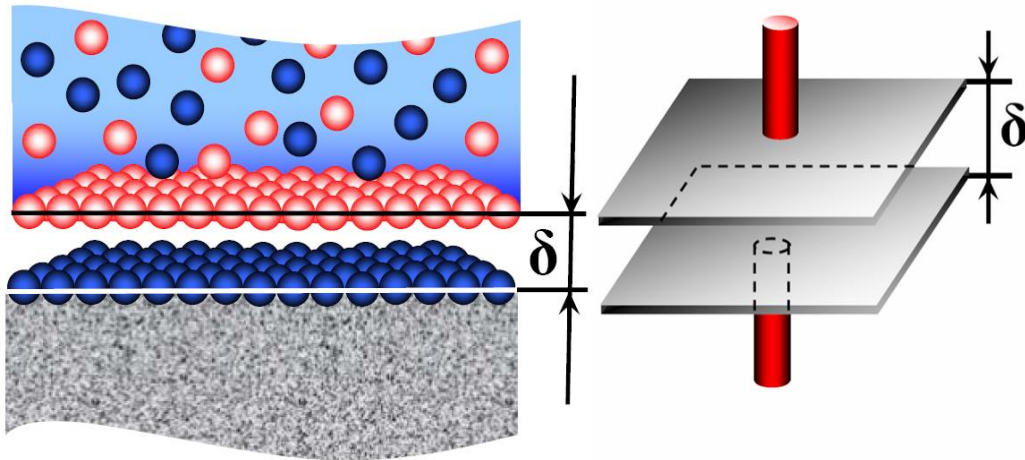


**Figure 18.** Schematic illustration of electric double layer arisen on the interface between the electrode's surface and the electrolyte.

From physical point of view, this electric double layer is potential barrier, and each ion from the bulk of the electrolyte should overcome it before to react with the elements from the metal surface.

In addition, every kind of covering dielectric layer on the electrode's surface possesses character of capacitance. For example, the native oxide layer on the aluminium, or whatever protective coating possesses capacitive resistance.

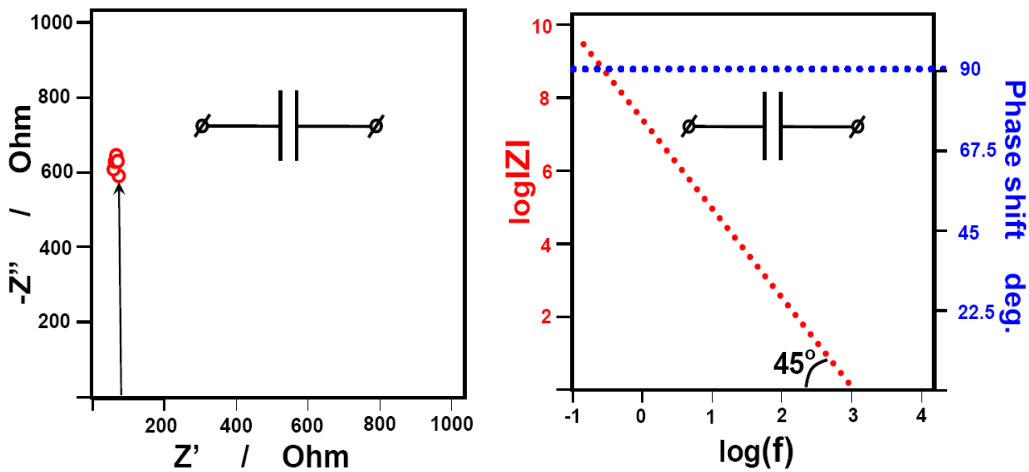


**Figure 19.** Nyquist and Bode plots of capacitive resistance

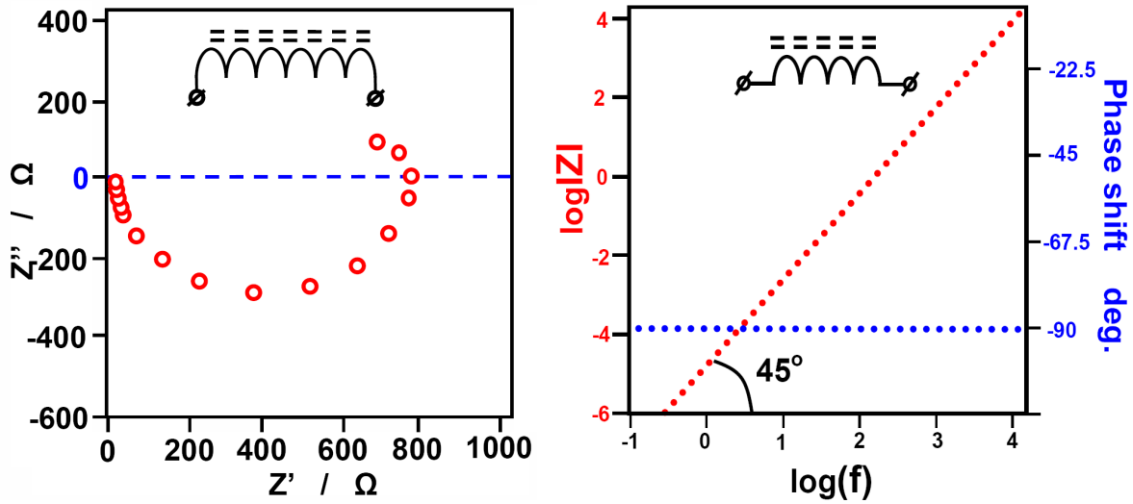


**Figure 20.** Nyquist (on the left) and Bode (on the right) plots of inductive resistance

- **Inductive reactive resistance:** The appearance of induction is relatively rare phenomenon. There is not agreement among the scientific investigators regarding its origin and nature. The explication of the nature of the inductive loops in an EIS spectra is rather contradictive. According to ref. [41], the presence of inductance is related to the presence of some anodic activity in the precipitates of Al(Cu,Mg). Other authors suggest that the inductive loop represents re-dissolving of previously passivated areas, which is notable at the lowest frequency part [42, 43]. The inductance has the expression on the impedance plots as is shown in Figure 20.

### 1.11. *Deviations of the spectra of the electrochemical cells from the electrotechnical electric circuits*

As it was mentioned above in the present text, the behavior of the electrochemical cells differs from this of the electric circuits. The difference is originated from the presence of electrochemical reactions on the surface of the electrodes, as well as from the fact that the charge transport through the electrolyte passes in form of charged ions, instead of electrons. Both of these reasons predetermine some considerable difference of the impedance spectra of the electrochemical cells, from the spectra of the electric circuits.

The first and the most frequently observed peculiar feature of the impedance of the electrochemical cells is that the phase shift between the sinusoids of the current (amperage) and the excitation potential (voltage) and could possess values different than 90°. In this case, the capacitive resistance of the cells is accepted as Constant Phase Elements (CPE), instead of pure capacitance.

The constant Phase Element (CPE) is conditional parameter for description of the cell's frequency dependent impedance. Its values could be accepted rather as capacitance, diffusion element, or resistance, conditionally, according to the value of the exponential multiplier "n". The value of its impedance could be determined, as follows:

$$\text{---} , \tag{29}$$

where:  $Z_{CPE}$  – is the impedance of CPE;  $Y_0$  is constant; n is exponential multiplier,  $\omega$  is the angular frequency, and j – is the imaginary value.

Certain physical significance of this conditional element could be ascribed to the constant  $Y_0$ , only at defined values of n, as follows:

- If  $n = 0$ , than the constant  $Y_0$  is considered as resistance, the values are measured as  $\Omega^{-1} = S$  (Siemens).
- If  $n = 0.5$ , than the constant  $Y_0$  possess significance of diffusion (Warburg) element, occupying the measuring unit of  $\Omega^{-1} s^{0.5}$ .
- If  $n = 1$ , than  $Y_0$  is considered as pure capacitive resistance, and its units are  $\Omega^{-1} s = F$  (Farad).

The reason for the presence of CPE is the electrochemical nature of the charge transfer reactions on the surfaces of the electrodes. It should be mentioned that the charge transfer is accompanied by chemical conversion (oxidation or reduction) due to the electrochemical nature of the electrode processes.

Another peculiar feature of the electrochemical cells is that the diffusion processes could be involved to the charge transport through the electrolyte. In the case of electrochemical cells, the charge carriers in the electrolyte are ions, thus their transport is driven by the laws of Fick for diffusion.

In order to model the diffusion processes, Graham (1958) invents the element  $Z_w$ , (Warburg impedance). According to the laws of Fick for diffusion the Warburg impedance has the following expression:

$$Z_w = \frac{\sigma}{\sqrt{\omega}} (1 - j), \quad (30)$$

where:  $\sigma$  – is Warburg’s constant,  $\omega$  – angular frequency;  $j$  – imaginary unit.

When very high frequencies are applied to given electrochemical cell, this stimulates the ions to vibrate around their positions. They vibrate following the oscillations of the electric field, and thus:  $\omega \rightarrow \infty, Z_w \rightarrow 0$  relations are valid. However, at enough low frequencies, the ions begin to perform “forward-backward” movements, which length corresponds to the amplitude.

The equation 30 reveals that the values of the real and the imaginary parts of Warburg impedance are equal. Due to that reason, in the complex plane of the Nyquist plots the Warburg impedance appears in form of straight line with slope equal to  $45^\circ$ .

### 1.12. *Modeling in the EIS. Equivalent circuits*

The principal way to approach the analysis of the EIS results is using the “equivalent circuit” concept. It stand on the fact that, in principle, any electrochemical cell may be represented by an electrical model.

The analysis of the impedance spectra represented in Nyquist and Bode plots is based on selection of appropriated models (equivalent electric circuits) and posterior fitting of the values of their active and reactive resistances to these of the acquired spectrum from EIS-measurement to the real electrochemical cell. According to Zheludkevich, [44] there are several basic equivalent circuits, which could be applied for fitting of EIS-spectra of corrosion of coated aluminium alloy. Each circuit is more appropriated for fitting of one or other stage of the corrosion. Figure 21 shows the respective basic equivalent circuits.

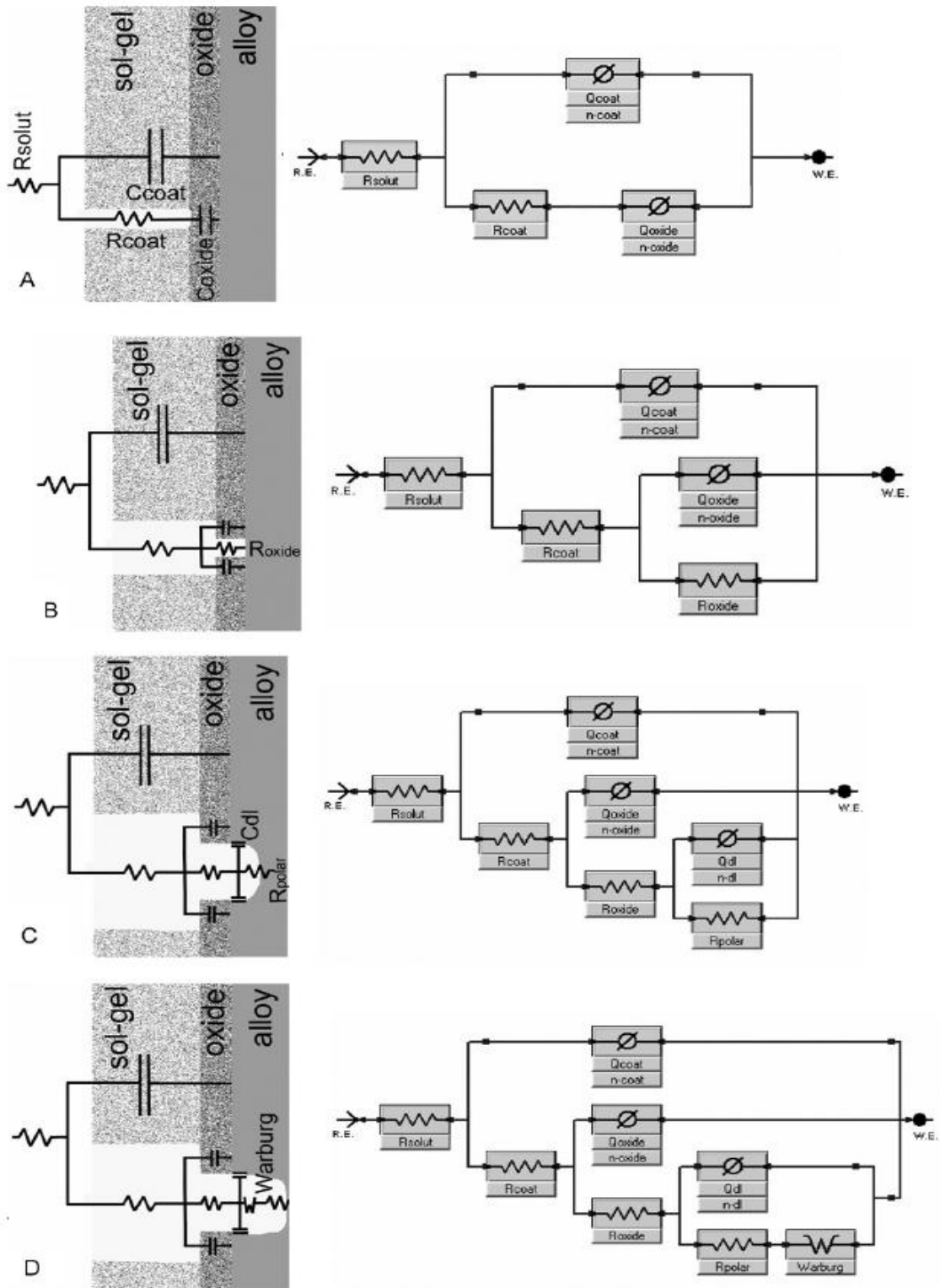


**Figure 21.** Equivalent circuits for description of different stages of corrosion of coated aluminium [44-45]. A- electrolyte penetration through the coating; B- electrolyte penetration through the oxide layer; C- Corrosion of the alloy; D- Corrosion, combined with diffusion of corrosion products.

### 1.13. Verification of the reliability of the EIS measurements and modeling

For verification of the data obtained either by the EIS measurement, or the quality of fitting, could be executed by the test of Kramers – Kroenig (K – K test) [46].

- *Direct application of K – K test to EIS measurements:* When it is applied for the measurement, then it reveals whether the measured data comply with the assumptions of Kramers – Kroenig. These assumptions are, as follows:

- The response (output signal between RE and WE) corresponds only to the excitation (input signal between CE and WE).
- Presence of linear dependence between the perturbation (input signal) and the response (output signal).
- Absence of notable changes of the electrochemical system during the measurements (the changes could be in the minimal limit of detection).

When the system does not relay to these requirements, then the test shows unsatisfying level of reliability. The possible reasons for deviation of the systems from the requirements of K-K test could be as follows: 1- Missing of stationary of the system (when its parameters suffer significant changes during the measurements) and 2- Change of external parameters of the environment (temperature, pressure, etc.).

The K –K test is based on fitting to special model equivalent circuit, composed by time constants, which number (n) is equal to the total number of the data points in the spectrum. The arrangement is represented in Figure 22 below:

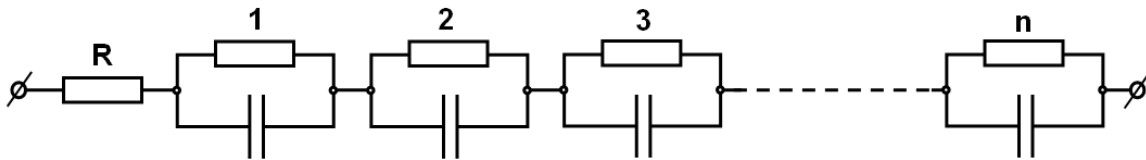


Figure 22. Equivalent circuit for K – K test .

- *Application of K – K test to fitting by equivalent circuit:* In the case of impedance modeling, the application of K – K test gives information about reliability of the equivalent circuit to the relevant impedance spectrum.

- *Quantitative criterion of K –K test:* The results of the test is a value, named pseudo"ksi" – square ( $\chi^2$ ), which is defined as sum of the squares of the relative residuals.

The value of the total  $\chi^2$  could be calculated as sum of the imaginary  $\chi^2$ , and the real  $\chi^2$ . Here, should be mentioned that the relatively large values of  $\chi^2$  correspond to relatively poor concordance between the measured impedance spectrum and the spectrum of the respective equivalent circuit, used for fitting. The assumption of pseudo  $\chi^2$  – as “small”, or “big”, is quietly relative. Generally, it depends on the number of the data points which compose the obtained EIS-spectrum.

As a conditional rule, it is accepted that when the  $\chi^2$  – value is lower than  $10^{-6}$ , than, the respective fitting is excellent. It could be accepted as “reasonable” at  $\chi^2$  is in order of  $10^{-5}$ ; “satisfactory”, when  $\chi^2$  is near to  $10^{-4}$ , and marginal at values of  $\chi^2$  higher than  $10^{-3}$ .

The values of  $\chi^2$  could be calculated, according to the following equation:

$$\text{-----} \tag{31}$$

$$\text{-----} \tag{32}$$

$$\text{-----} \tag{33}$$

$Z_{re,i}$  and  $Z_{im,i}$  – are the measured imaginary and real components of the impedance spectrum.

$Z_{re,(oi)}$  and  $Z_{im,(oi)}$  – are the imaginary and real components owned by the respective equivalent model circuit.

Detailed description over the K – K test, and its theoretical bases are discussed in detail by Dr. B. A. Boukamp in ref. [47].

#### 1.14. Equipments and methods for surface observations:

Two basic equipments for surface observations were used for the study of the present work: Optical Microscopy and Scanning Electronic Microscopy

- **Optical microscopy:** This kind of microscopy is the oldest known method, for observation of microscopic object. It is invented in XVI century by Antoni Vant Loevenhuck, who has described for first time the observation of very small organisms in a drop of rain water. This method is based on acceleration of the images, obtained by interaction between the light and microscopic object.

The optical microscopes could be divided into two general groups, according the nature of the interactions between the light and the observed object:

*Microbiologic* – The observed image is obtained by the transmitted through the object light.

*Crystallographic* – There, the observed images are consequence of refracted by the surface light.

Figure 22 shows a typical microbiologic microscope. Its construction differs from this of the crystallographic microscopes by the place of the light source.

The basic parameters of the microscopes are as follows:

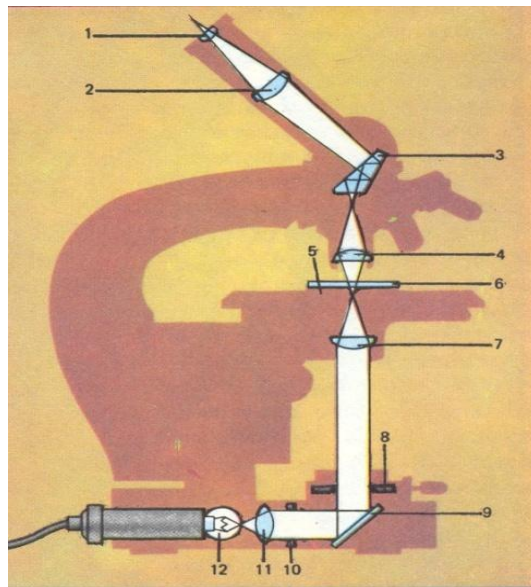


**Figure 23.** Microbiologic Optical Microscope [46]

1-2. Eye-lenses; 3. prysm; 4. Object lense ;5. Sample holder; 6. Sample  
7 - 11. Light fixing lense; 8-10. Blinds; 9. Refractor; 12. Light source

Two important characteristics for these kind of microscopes could be marked, namely: (i)- *Resolution rate*: The lowest distance between two points, which could be distinguished and (ii)- *Image acceleration rate*: Shows how much times the image is accelerated .

- ***Scanning electronic microscopy***: Is developed as successor of the earlier Transmission Electronic Microscopy (TEM). The electronic microscopy is based on the interaction between the particles composing the surface of the object of observation, and accelerated electronic beam. Through the collision of the electrons of the beam with the particles composing the sample, various derivative radiations could be observed.

Generally the electron microscopes could be described as vacuum tubes, where several basic elements are mounted:

- Electronic emitters: They are composed by tungsten electric heater, electric plate (cathode), which is connected to high voltage system, and electron's accelerator (an electrode with form of ring or cylinder).
- System of capacitive and electromagnetic "lenses": They are mounted through the path (from the emitter to the probe's surface) of the electronic beam. Their function is to control the acceleration of the electronic beam, and to control its diameter.
- Systems of detection: They reproduce the image obtained by the interactions between the electrons from the beam, and the particles composing the surface of the sample. These systems detect all of the derivative radiations, as:
  - a) Secondary electrons: They are turned out from the electronic shells of the atoms from the sample, by collisions with the electronic beam.
  - b) Back scattered electrons: They are "refracted" electrons from the beam, by the collisions with the sample's surface.
- X-ray characteristic photoemissions: When an electron from the beam collides with one of the electronic shell of atom of the sample, the latter electron accepts the kinetic energy from the former (occupying the higher energetic

level). Afterwards, it returns to its basic energetic level, transmitting X-ray photon.

Figure 24 shows a schematic view of the distribution form of derivative radiations, provoked by the collisions between the electrons of the electronic beam and the solid sample's surface.

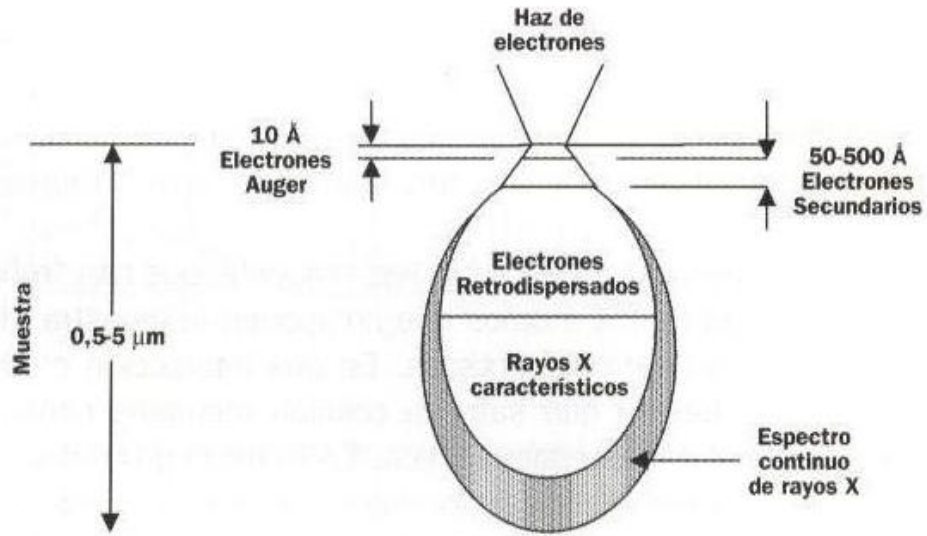


**Figure 24.** Schematic view of the penetration of electronic beam into a solid sample, and the respective derivative emissions [49]

## II. AIMS OF STUDY

### 2. Propose of experimental work

Some comparisons of inhibitor's efficiencies of Ce(III) and Ce(IV) ammonium nitrates were done for aluminium alloys like AA3003 and AA6063, it was established that the composition of the aluminium alloy has significant importance. Any similar comparative investigations regarding the inhibition efficiency of Ce(III) and Ce(IV) ions against the corrosion of one of the most widely used alloys AA2024 is not found in the literature. So, the aim of the present work is to evaluate the inhibitive efficiency of Ce(III) and Ce(IV) ions against the corrosion of the AA2024 alloy in 3.5% NaCl solution.

To calculate the inhibition efficiency of Ce(III) and Ce(IV) for aluminium alloy AA2024 both of ions were introduced in the solution in form of cerium salts with similar anionic compositions -  $(\text{NH}_4)_2\text{Ce}(\text{NO}_3)_5$  and  $(\text{NH}_4)_2\text{Ce}(\text{NO}_3)_6$ . The latter salt has found good application in chemical analytical practice. It was established that a small part of Ce(IV) ions is always represented in the solution in form of anionic complexes [50]. This fact additively enhances the interest to this salt. Moreover, the inhibition ability is planning to investigate with diverse concentrations of the two ions in the corrosive media and also at different exposition time (2, 4, 24, 72 and 120 hours ) i.e. durability tests execution. The pH values of the solutions were also determined. For achievement of the basic aim of the present research two electrochemical techniques will be applied: Linear Voltammetry (LVA), and Electrochemical Impedance Spectroscopy (EIS). The results obtained from the electrochemical measurements will be confirmed by observations of the surface morphology via two techniques: Scanning Electronic Microscopy and Optical Microscopy.

### III. EXPERIMENTAL

#### 3. Objects of research:

##### 3.1. Description of the objects of research

The objects of research of the present work are five bare samples of AA2024, exposed to standard corrosive medium represented by 0.6 M of NaCl, with different concentrations of Ce(III)- and Ce (IV)- Ammonium Nitrate in the corrosive media.

The composition of the alloy was additively analyzed by Inductively Coupled Plasma - Optical Emission Spectroscopy (ICP-OES) according to a standard analytical route, after dissolution in acidic media. The data obtained are presented in Table 3.

**Table 3.** Composition of the AA2024 alloy, analyzed by ICP OES.

Element	Cu	Fe	Mg	Mn	Ni	Si	Al
Content (wt. %)	3.716	0.404	1.259	0.537	0.055	<0.01	Balance

The respective concentrations of the both inhibitors Ce(III) and Ce(IV) in the corrosive medium were, as in the following table:

**Table 4.** Inhibitor's concentration for the corresponding corrosive media

Code	Concentration (M)
A000M	Reference
A102M	$1 \times 10^{-2}$
A103M	$1 \times 10^{-3}$
A104M	$1 \times 10^{-4}$
A105M	$1 \times 10^{-5}$

### 3.2. *Methods and equipment of measurements:*

Select samples of the alloy have been preliminary treatment by grinding with emery paper of 200, 360, 500 and 800 grits. After that subsequent degreasing by ethanol : ether (1 : 1) mixture, followed by vigorous cleaning by distilled water were done.

In order to perform the electrochemical measurements, a flat three-electrode cell with 100 ml volume was used. Limited zones of the metals plates in form of circuits with 2 cm<sup>2</sup> area, exposed to the corrosive medium served as Working Electrodes (WE). The counter electrode was a platinum net with cylindrical form, which surface area was at least two orders of magnitude higher than this one of the working electrode. The electrochemical measurements were performed in respect to a commercial Ag/AgCl 3 M KCl electrode, model 6.0733.100, product of Metrohm (Netherlands). The model corrosive medium was 3.5 % NaCl solution. All measurements were done at room temperature. The polarization curves were recorded by Potentiostat/Galvanostat PGStat Autolab 30, product of Ecochemie (Netherlands). The impedance spectra were acquired by an additive Frequency Response Analyser (FRA-2), product of the same producer. In order to avoid external static electrical field influences, the entire cell was shielded in a Faraday cage. Figure 25 illustrates the schematic presentation and real photography of the used cells:

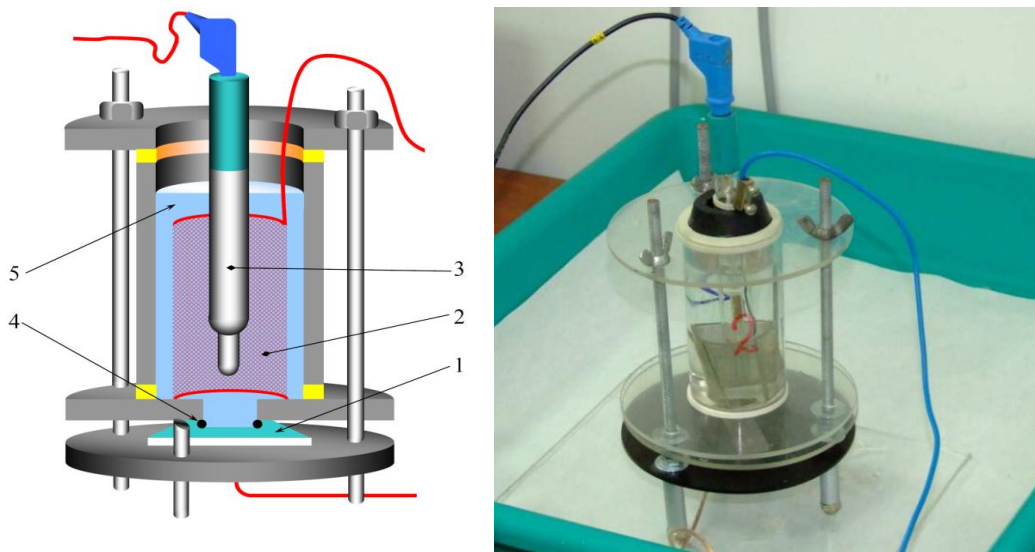


**Figure 25.** Schematic view (a), and photograph (b)

1 – Working electrode; 2 – Counter electrode; 3 – Reference electrode; 4 – protective gasket; 5 – electrolyte

### 3.3. *Electrochemical measurements*

In order to minimize the polarization of the working electrode, the electrochemical measurements were performed in the following subsequence: the initial polarization curves were recorded two hours after exposure of the samples to the corrosive medium. They were acquired in a narrow interval around the Open Circuit Potential ( $OCP \pm 0.030$  V), with potential sweep range 1.0 mV/s. The values of  $R_p$  and  $E_{corr}$  were determined on the base of these curves. The difference between the values of OCP and  $E_{corr}$  obtained by these measurements, were not superior to 1-2 mV. Afterwards, the respective impedance spectra were acquired at the following conditions: Frequency range: from  $10^4$  to  $10^{-2}$  Hz, distributed in 7 frequencies per decade, with a signal amplitude 10 mV according to OCP. At last, individual cathodic and anodic polarization curves were recorded in a larger potential's interval: : from OCP to -500 mV, for the cathodic curves and from OCP to +500mV for the anodic curves, respectively. In both cases the potential sweep range was 1 mV/s. By maintenance of this sequence, any disgrace of the experimental data as consequence of electrode polarization could not be admitted.

Two cerium salts were used for corrosion inhibition;  $(NH_4)_2Ce(NO_3)_5$  and  $(NH_4)_2Ce(NO_3)_6$ , where the cerium is in third and fourth oxidation states, respectively. Additions of each salt with concentrations;  $10^{-2}$ ,  $10^{-3}$ ,  $10^{-4}$  and  $10^{-5}$  M to the corrosive medium were done. The pH values of the solutions were determined by HI 255 combined meter, produced by Hanna Instruments.

### 3.4. *Topographic observations*

Two equipments were employed for topographic observations:

- *Optical microscopy*: It was done by binocular, revolver microscope, produced by Boeco – Germany. Image magnification was 100 times, connected with a web-camera.
- *Scanning electronic microscopy*: the experiments were performed by JEOLS 35G, scanning electronic microscope from JEOL – Japan.

## IV. RESULTS OF MEASUREMENTS:

### 4. Results obtained

#### 4.1. *Equivalent circuit employed for the object of research*

As was described above (see section 2.1) the present work has motivation to investigate the behavior of AA2024, exposed to corrosive medium with different amount of Ce- base inhibitor (see Table 4). That behavior was assessed via Electrochemical Impedance Spectroscopy. The results obtained were verified by Linear Voltammetry. The impedance spectra were analyzed by modeling through fitting procedure applying appropriated equivalent electric circuit.

The experimental data obtained have been fitted by equivalent circuit, which was a modification of the circuits proposed by Zheludkevich [44] (see Fig. 21) At that case, high goodness rate ( $\chi^2$ ) possesses values from  $10 \times 10^{-3}$  to  $3 \times 10^{-3}$ , and it was achieved by use of the equivalent circuit shown in Figure 26:

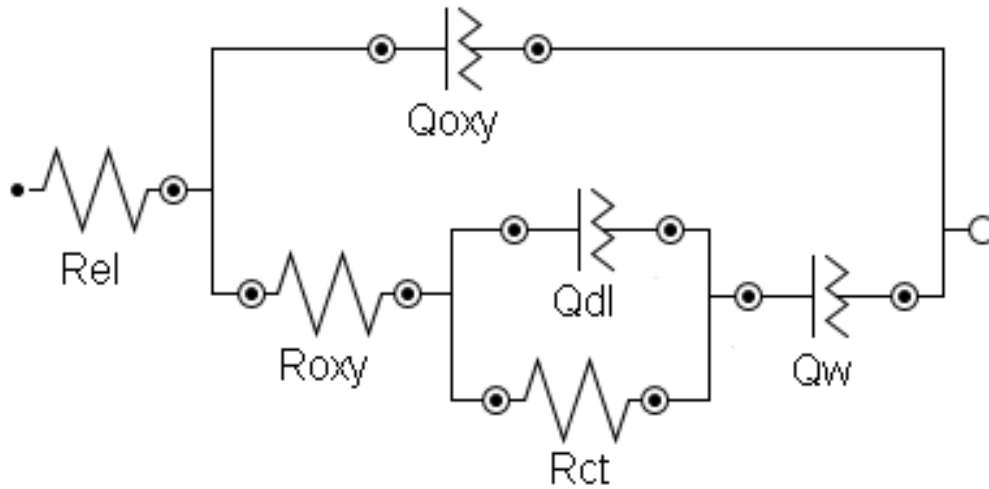


**Figure 26.** Equivalent circuit, used for fitting of the experimental data; where  $R_{el}$  – electrolyte's resistance;  $Q_{oxy}$  – Constant Phase Element of the oxide layer;  $R_{oxy}$  – Resistance of the oxide layer;  $Q_{ct}$  - Constant Phase Element of the charge transfer;  $R_{ct}$  – Resistance of the charge transfer;  $Q_w$  - Constant Phase Element for diffusion

#### 4.2. Application of Modeling by equivalent electric circuits

The results obtained via fitting procedure for Ce (III) and Ce(IV) – inhibitors are summarized in Tables 5 and 6, respectively.

**Table 5.** Results obtained via fitting for Ce(III), concentration:  $1 \times 10^{-4}$  M

Ce(III) $10^{-4}$ M pH= 5.38			
Element (unit)	4h	24h	72h
$R_{el}$ ( $\Omega \cdot \text{cm}^2$ )	7.21	7.28	7.23
$Q_{oxy} 10^{-5}$ ( $\text{s}^n \cdot \Omega^{-1} \cdot \text{cm}^{-2}$ )	6.37	4.58	4.88
$n_{oxy}$ (/)	0.869	0.890	0.885
$R_{oxy}$ ( $\text{k}\Omega \cdot \text{cm}^{-2}$ )	19.67	9.14	4.91
$Q_{dl} 10^{-5}$ ( $\text{s}^n \cdot \Omega^{-1} \cdot \text{cm}^{-2}$ )	0.447	0.270	2.05
$n_{dl}$ (/)	0.859	1.000	0.95
$R_{ct}$ ( $\text{k}\Omega \cdot \text{cm}^2$ )	33.3	17.50	6.51
$Q_w 10^{-3}$ ( $\text{s}^n \cdot \Omega^{-1} \cdot \text{cm}^{-2}$ )	2.80	3.92	9.08
$n_w$ (/)	0.780	0.942	0.72
$\chi^2 10^{-3}$ (/)	5.364	5.775	9.437

**Table 6.** Results obtained via fitting for Ce(IV), concentration:  $1 \times 10^{-5}$ 

Ce(IV) $10^{-5}$ M pH= 5.35			
Element (unit)	4h	24h	72h
$R_{el}$ ( $\Omega.cm^2$ )	8.23	8.78	6.93
$Q_{oxy} 10^{-5}$ ( $s^n.\Omega^{-1}.cm^{-2}$ )	8.10	1.95	6.32
$n_{oxy}$ (/)	0.847	0.818	0.870
$R_{oxy}$ ( $k\Omega.cm^{-2}$ )	4.53	1.66	5.50
$Q_{dl} 10^{-5}$ ( $s^n.\Omega^{-1}.cm^{-2}$ )	0.905	4.56	3.26
$n_{dl}$ (/)	1.0	0.893	0.831
$R_{ct}$ ( $k\Omega.cm^2$ )	14.04	14.98	5.170
$Q_w 10^{-3}$ ( $s^n.\Omega^{-1}.cm^{-2}$ )	2.45	1.91	1.040
$n_w$ (/)	0.820	0.670	0.340
$\chi^2 10^{-3}$ (/)	10.20	3.772	9.290

**4.3. Results obtained by polarization curves:**

**Table 7.** Rp for AA2024 after different time of immersion in 3.5% NaCl solution, with and without Ce(III) ammonium nitrate inhibitor additions.

	Ce(III) amm. Nitrate	pH	2h		4h		1D		3D		5D	
			OCP	Rp	OCP	Rp	OCP	Rp	OCP	Rp	OCP	Rp
1	0.0 M	6.50	-0.943	6.77E+3	-0.908	9.953E+3	-0.915	8.861E+3	-0.91	1.119E+4	-0.887	2.017E+4
2	10 <sup>-2</sup> M	3.10	-1.043	1.47E+3	-0.951	1.383E+3	-0.667	8.013E+2	-0.69	5.797E+3	-0.70	3.565E+3
3	10 <sup>-3</sup> M	4.20	-0.934	2.956E+4	-0.844	3.751E+4	-0.949	1.874E+4	-0.91	3.05E+4	-0.829	4.719E+4
4	10 <sup>-4</sup> M	5.38	-0.955	3.025E+4	-0.91	4.638E+4	-0.991	2.609E+4	-1.039	1.178E+4	-0.882	3.21E+4
5	10 <sup>-5</sup> M	6.45	-0.928	1.964E+4	-0.916	2.531E+4	-0.994	3.542E+4	-1.073	8.307E+3	-0.98	1.22E+4

**Table 8.** Rp for AA2024 after different time of immersion in 3.5% NaCl solution, with and without Ce(IV) ammonium nitrate inhibitor additions.

	Ce(IV) amm. Nitrate	pH	2h		4h		1D		3D		5D	
			OCP	Rp	OCP	Rp	OCP	Rp	OCP	Rp	OCP	Rp
1	0.0 M	6.50	-0.943	6.77E+3	-0.908	9.953E+3	-0.915	8.861E+3	-0.91	1.119E+4	-0.887	2.017E+4
2	10 <sup>-2</sup> M	1.72	-0.79	2.398E+2	-0.816	3.971E+2	-0.696	6.378E+2	-0.634	2.605E+1	-0.725	2.514E+2
3	10 <sup>-3</sup> M	2.69	-1.016	8.388E+2	-0.990	9.915E+2	-0.816	1.57E+3	-0.689	7.808E+2	-0.692	4.48E+2
4	10 <sup>-4</sup> M	3.71	-0.882	5.956E+3	-0.869	1.232E+4	-0.904	1.248E+4	-0.912	1.583E+4	-0.862	2.319E+4
5	10 <sup>-5</sup> M	5.35	-0.927	1.872E+4	-0.880	2.343E+4	-0.944	1.767E+4	-0.988	1.317E+4	-0.844	3.222E+4

## V. DISCUSSIONS OF THE RESULTS OBTAINED

### 5. Results and discussions

#### 5.1. *EIS measurements*

The electrochemical impedance spectroscopy (EIS) enables to distinguish the processes in the interfaces metal / oxide layer / electrolyte of the electrochemical systems. In addition, the clarification of these processes, their quantitative assessment, as well as the characterization of their evolution within the exposure time could be done by the application of modeling. The last one could be executed by fitting procedure with appropriated equivalent circuits, according to the discussion carried out in the theoretical part of the present work.

Figures 27, 28, 29 and 30 summarize the Nyquist and Bode plots of the impedance spectra and their evolution within the time of the samples exposition in the corrosive media, containing Ce(III) or Ce(IV) ions. The spectra obtained for both of Ce(III)- and Ce(IV)- ions are recorded for solutions with similar pH values (pH = 5.38 for Ce(III) ions and pH = 5.35 for Ce(IV) ions). These predominate and stimulate an adequate interpretation of the results obtained.

As evidently is from Figures 27 and 29 the Nyquist plots are composed by one unique depressed capacitive semi-circle, which is result of superposition of two time constants. They could be ascribed to the presence surface oxide layer, and charge transfer between the liquid corrosive medium and the metal surface.

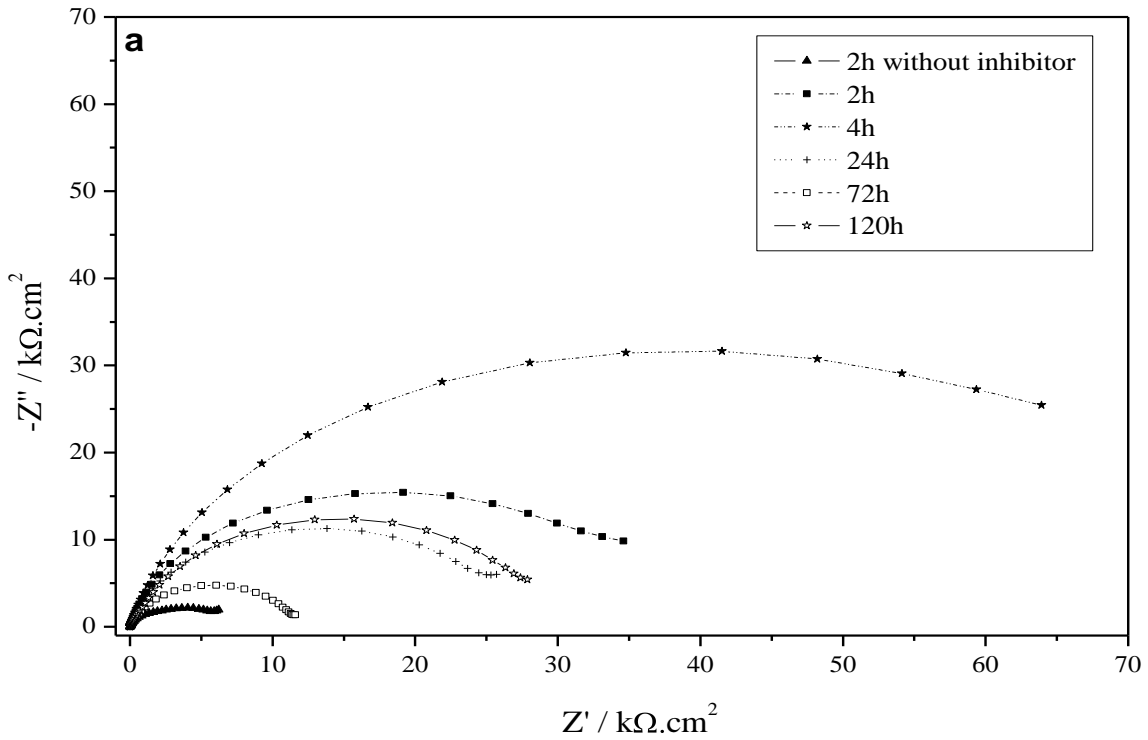


**Figure 27.** Nyquist plot of the impedance spectra and their evolution within the time of exposition of the samples in the corrosive medium for Ce(III) 104 M

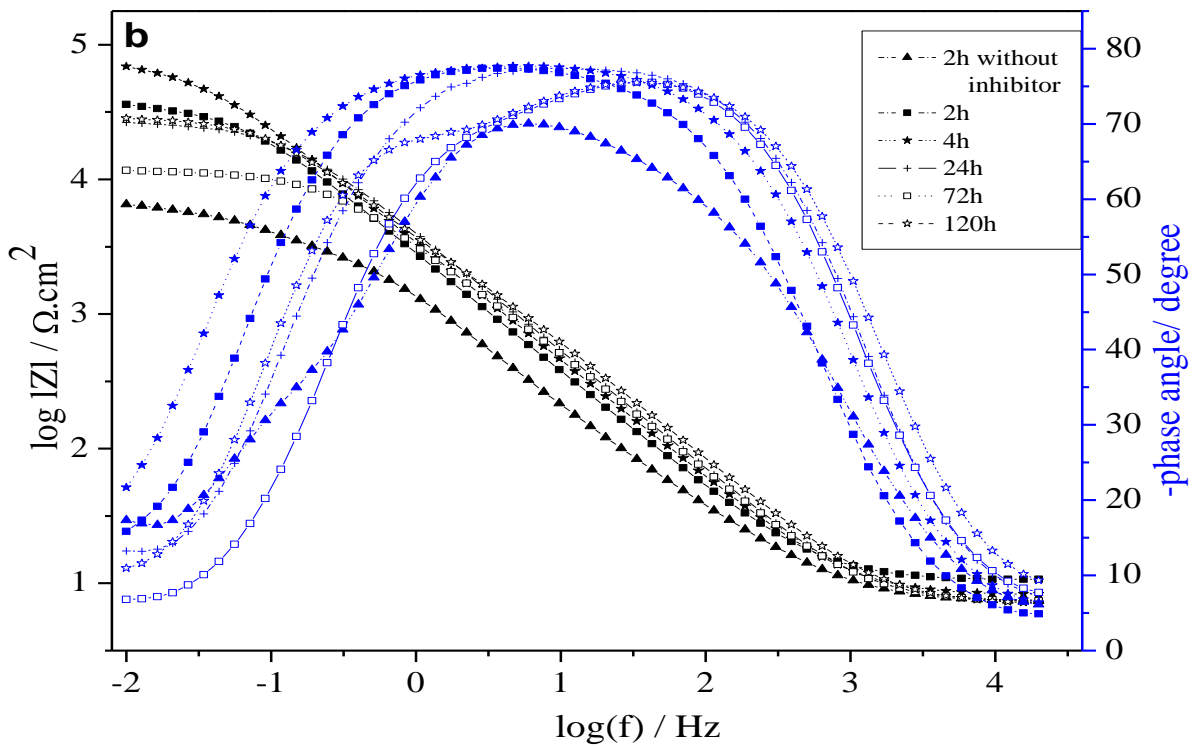


**Figure 28.** Bode plot of the impedance spectra and their evolution within the time of exposition of the samples in the corrosive medium for Ce(III) 104 M

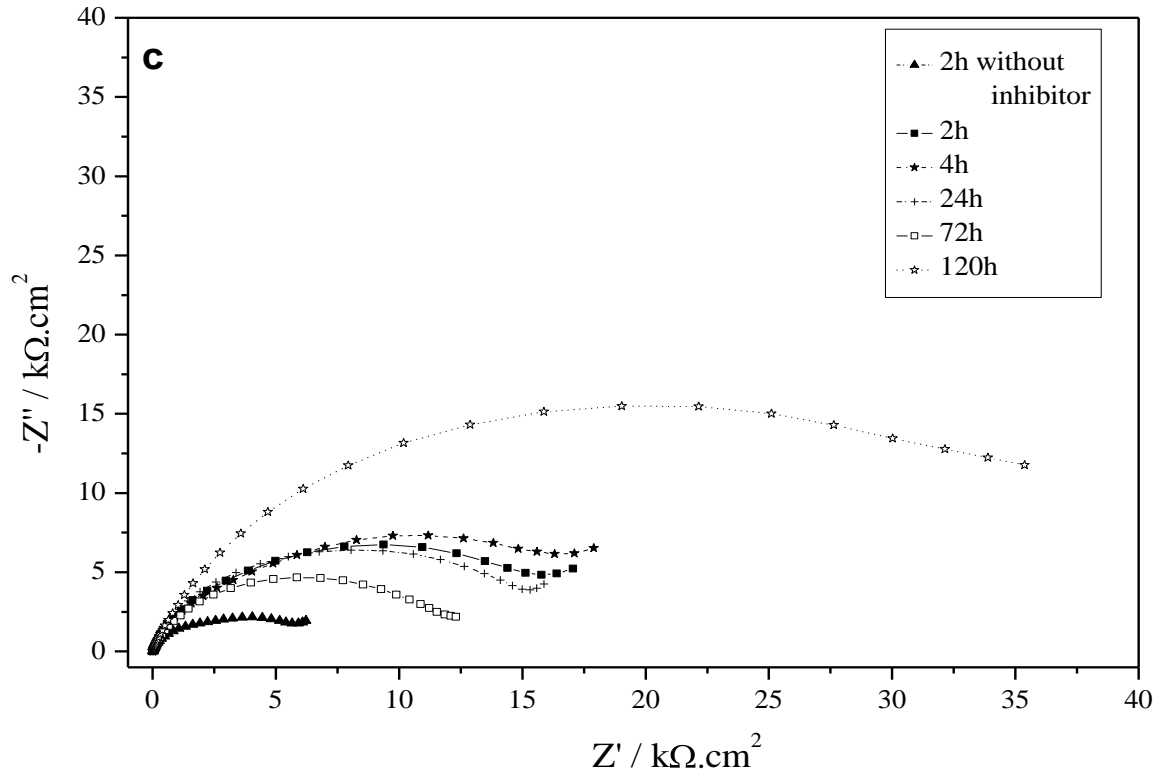


**Figure 29.** Nyquist plot of the impedance spectra and their evolution within the time of exposition of the samples in the corrosive medium for Ce(IV) 105 M

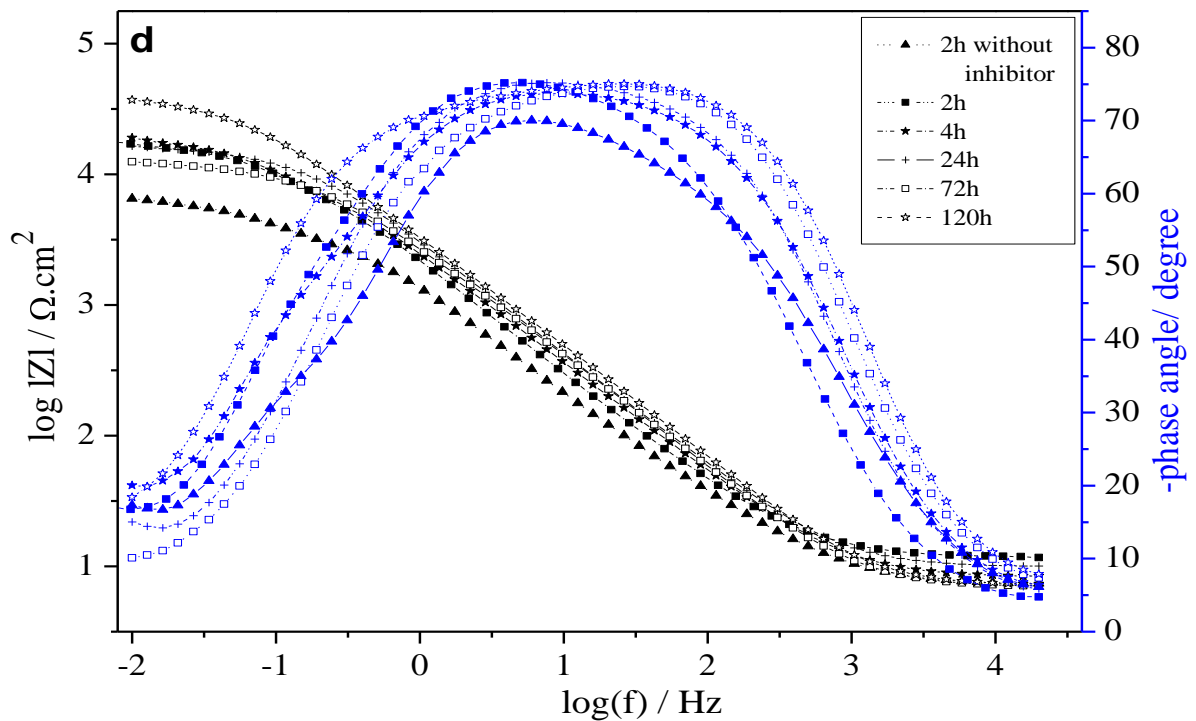


**Figure 30.** Bode plot of the impedance spectra and their evolution within the time of exposition of the samples in the corrosive medium for Ce(IV) 105 M

## 5.2. EIS modelling

For quantitative interpretation of the data obtained by EIS spectra, a structural impedance modeling was performed. It was realized by fitting of the respective experimental spectra to appropriate equivalent circuit. Figure 25 represents the equivalent circuit used for fitting in the present research. The equivalent circuit in the present work is in accordance to the basic ideas, described by Boukamp [47].

After the analysis of the data obtained for  $R_{ct}$  and  $R_{oxy}$  of Ce (III) ammonium nitrate (Table 5), the corresponding parameters for Ce (IV) ammonium nitrate, (Table 6), and their polarization resistances (Tables 7 and 8, respectively), it was discovered that the values of  $R_p$  always correspond to the sum between  $R_{ct}$  and  $R_{oxy}$ , i.e. we have full correlation effect with equation (34). It reveals clear accordance between the data obtained by the impedance measurements and the results acquired by the polarization curves. In addition, the remarkable advantage of the impedance technique is that it enables to discover the structure of the polarization resistance  $R_p$ , obtained by the method of the linear Voltammetry, in the cases of passivated systems. It is composed by two parts: resistance of the charge transfer across the metal/electrolyte interface  $R_{ct}$  and the resistance of the oxide layer  $R_{oxy}$ , as is shown in equation (34)

$$R_p = R_{ct} + R_{oxy} \quad (34)$$

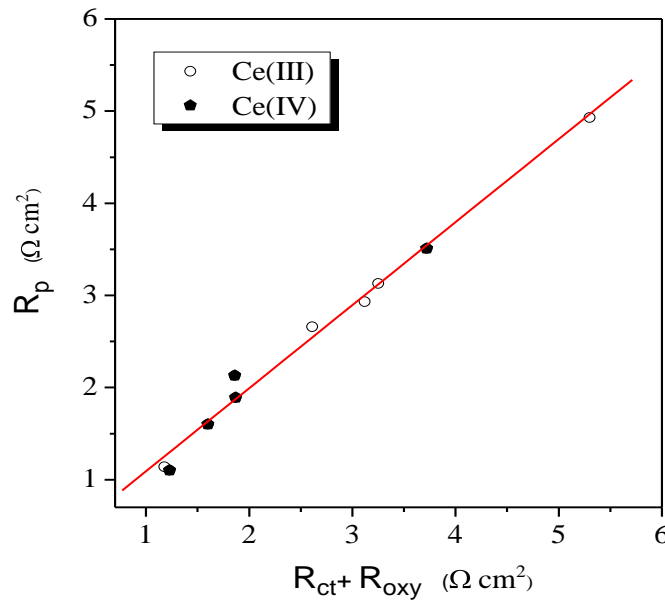


**Figure 31.** Correspondence of  $R_p$  values versus  $R_{ct} + R_{oxy}$

Figure 31 shows the correspondence of  $R_p$  values versus  $R_{ct} + R_{ox}$ . The straight line with slope equal to  $45^\circ$ , confirms the relation (34), and in addition it is a good agreement for the high accuracy of the electrochemical measurements done.

### 5.3. *Polarization measurements*

The polarization measurements enable to define a large number of important characteristics of the corrosion processes, such as the character of the inhibition effect, the inhibitor's efficiency, etc.

Figure 32 shows the cathodic polarization curves for different concentrations of Ce(III) and Ce(IV) ions, acquired after 24 hours of samples exposed into 3.5 % NaCl solution. For comparison, the cathodic polarization curve of the same alloy exposed to the corrosive medium in absence of the inhibitor is also represented.

It can be seen that for both Ce ions added at higher concentrations, (Ce(III) -  $10^{-2}$  M, Ce(IV) -  $10^{-2}$  and  $10^{-3}$  M), the cathodic currents are higher than that without inhibitor solution, when they are compared at defined value of the potential. Consequently, at these concentrations, the inhibitors act as activators. On the other hand, at lower concentrations of both Ce ions, the cathodic currents are lower than that of the referent solution. Simultaneously, the corrosion potential shifts to negative direction, compared to these of the reference. Such behaviour is typical for the cathodic inhibitors, reported in ref. [51, 52]. They retain the partial cathodic reaction and consequently the entire corrosion process.

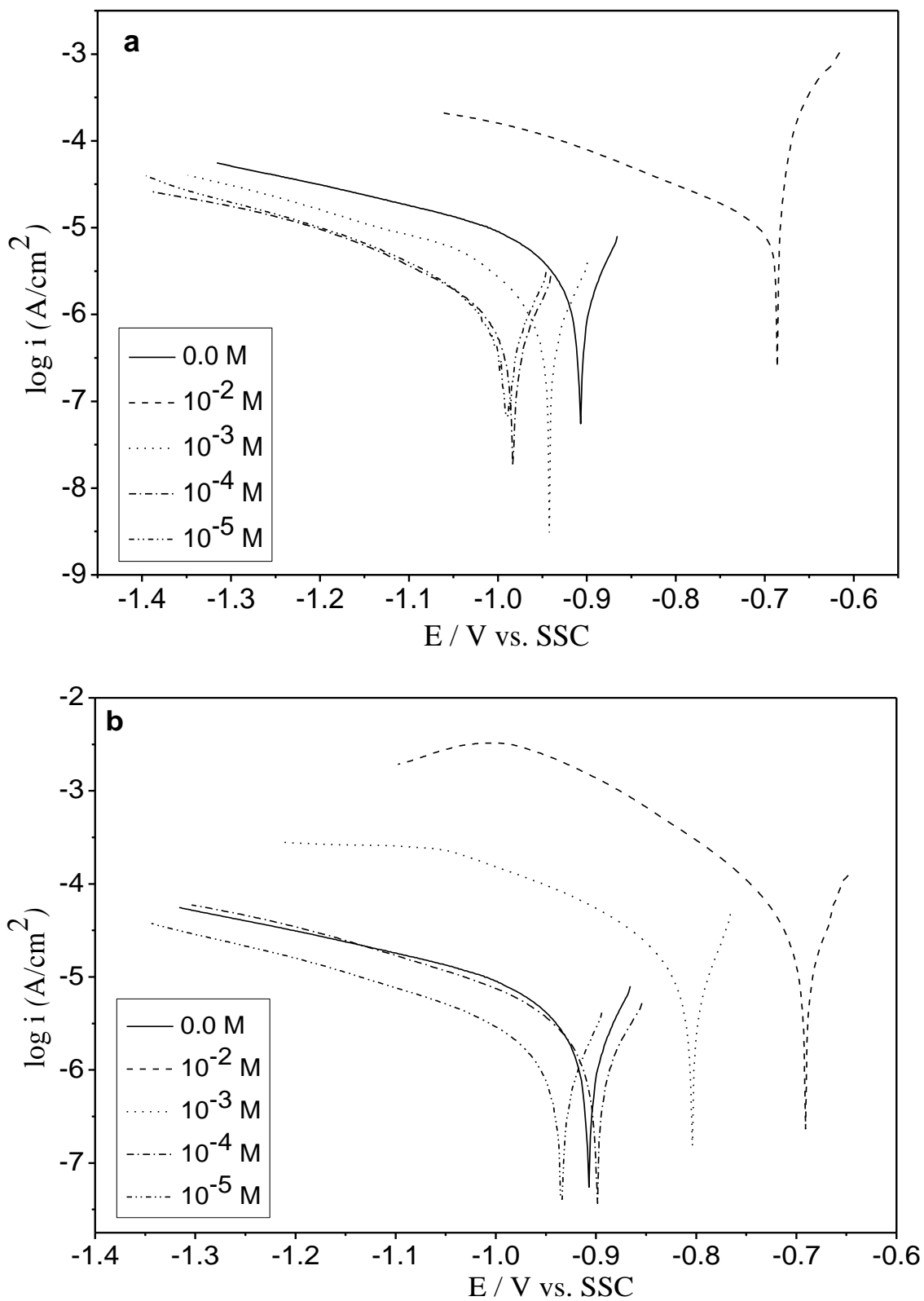


**Figure 32.** Cathodic polarization curves of AA2024 aluminium alloy, after 24 hours of exposure in 3.5% NaCl solutions with additions of different concentrations of; a)- Ce(III) and b)- Ce(IV)

A surprising effect can be checked, when the currents are higher, (more intensive corrosion), the  $E_{\text{corr}}$  potentials are nobler. It could be explained by the idea that at more intensive cathodic corrosion reactions, higher quantities of corrosion products are produced. They cover the anodic zones of the sample's surface, in form of sediments. Another possible explication for this effect is that the more intensive cathodic corrosion processes, lead to quick expense of the more active elements, composing the anodic zones of the alloy. Consequently, the  $E_{\text{corr}}$  of the alloy occupies nobler values of the potential.

The activation or inhibition effects of the cerium salts at different concentrations could be explained, when the ability of the cerium salts to hydrolyze in aqueous media is taken in account. Their hydrolysis leads to increase of the acidity of the media [3].

Table 9 contains data for the measured pH of the solutions, prepared by different contents of Ce(III) or Ce(IV) ammonium nitrates in 3.5 % NaCl medium.

**Table 9.** pH values for solutions of 3.5 % NaCl with different concentrations of Ce (III) and Ce (IV) ions

Oxidation state	Concentration (M)				
	0	$10^{-5}$	$10^{-4}$	$10^{-3}$	$10^{-2}$
pH at Ce(III)	6.50	6.45	5.38	4.20	3.10
pH at Ce(IV)	6.50	5.35	3.71	2.69	1.72

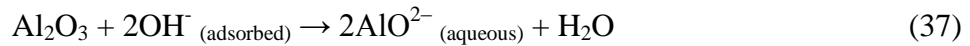
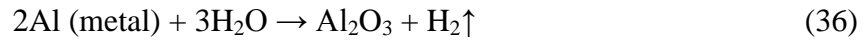
The sign is used for these values of pH, where both of ions reveal corrosion stimulation ability

The table shows that with increasing of the inhibitor concentration for both of the salts stimulating a significant decrease of the pH values. This decrease is more remarkable for the Ce (IV) ions. The lowest pH value is equal to 1.72 and belongs to the  $10^{-2}$  M solution of  $(\text{NH}_4)_4\text{Ce}(\text{NO}_3)_6$ . At this low value of pH, the surface oxide layer dissolves and the corrosion process passes as uniform corrosion. However, in neutral and weakly acidic media, the oxide layer is durable. At these conditions, the uniform corrosion is predominated by the local corrosion attack. The latter occurs on local areas of the alloy's surface.

The mechanism of the local corrosion of copper containing aluminium alloys is investigated by different authors [3, 53, 54]. It has been shown that the intermetallic particles with composition  $\text{Al}_2(\text{CuMg})$ , locked in the surface structure of the alloy, become centers of local corrosion. On the boundaries of such centre, a microgalvanic element arises, where the copper enriched areas becomes to be cathodic areas and the conjugated partial reaction of oxygen reduction occurs, as is described in detail [3, 53].



As result of reaction (35), the local pH value begins to increase and the oxide film together with the matrix around the intermetallic begins to dissolve [54]. It can be accomplished according to the following reaction:



In the presence of ions of Rare Earth elements (cerium ions),  $\text{OH}^-$  ions form oxides and hydroxides which possess remarkably low solubility. The last precipitate on the surface of the cathodic areas, retarding the rate of the oxygen reduction reaction (35). It was reported [55] that the solubility of  $\text{Ce}(\text{OH})_3$  is equal to  $1.6 \times 10^{-20}$ , while for  $\text{Ce}(\text{OH})_4$  is equal to  $2 \times 10^{-48}$ . As result, the conjugated anodic reaction of aluminium dissolution is retarded as well. By that manner, the entire corrosion process is hindered.

It is established that the pH of the solutions plays an important role on the inhibition process of the two cations. At high concentrations, both inhibitors lost their inhibition ability and start to act as stimulator of the corrosion process. This effect can be explain by the following manner, at high concentrations of the inhibitors, the solutions become more acidic (the pH decreases) and the oxygen reduction, according to the reaction (35) which is possible only in neutral and weakly acidic media, is hindered. In these cases, the cathodic processes begin to be dominated by another reaction which is described below:



According to that reaction, at the local corrosion centers any OH<sup>-</sup> ions does not generate and consequently, the formation of oxides of Ce ions is not probable anymore. In these conditions, especially for the solutions of Ce(IV) ions, another process begin to be also possible as a cathodic half reaction:



It involves an additive contribution in the rising of the cathodic currents in the polarization curves, recorded for the solutions of Ce(IV) with concentrations 10<sup>-2</sup> and 10<sup>-3</sup> M (Fig. 32b). The concentration of Ce-ions and pH of the medium predetermine which one of the parallel partial cathodic reactions (equations from 1 to 5), should dominate. However in all cases, the precipitates are being formed on the cathodic centers of the alloy surface. These precipitates are probably composed by mixtures of the oxides and hydroxides of both Ce(III), and Ce(IV) ions. On the base of the polarization measurements recorded in a narrow interval around the Open Circuit Potential (OCP ± 0.03 V), a quantitative data could be acquired. The corresponding curves enable determination of the polarization resistance R<sub>p</sub> values, and their evolution within the exposure time, avoiding any undesirable electrode polarizations.

The values of R<sub>p</sub> were used for calculation of the inhibitor's efficiency IE% at different concentrations of both cerium salts, according the equation below [56 – 60]:

$$\text{---} \quad (40)$$

Where R<sub>p</sub><sup>0</sup> is the polarization resistance in absence of the inhibitor and R<sub>p</sub><sup>inh</sup> corresponds to the polarization resistance in presence of the inhibitor with the corrosion medium.

Using the values from Tables 7 and 8, it was possible to calculate the inhibitor's efficiency by equation (40):

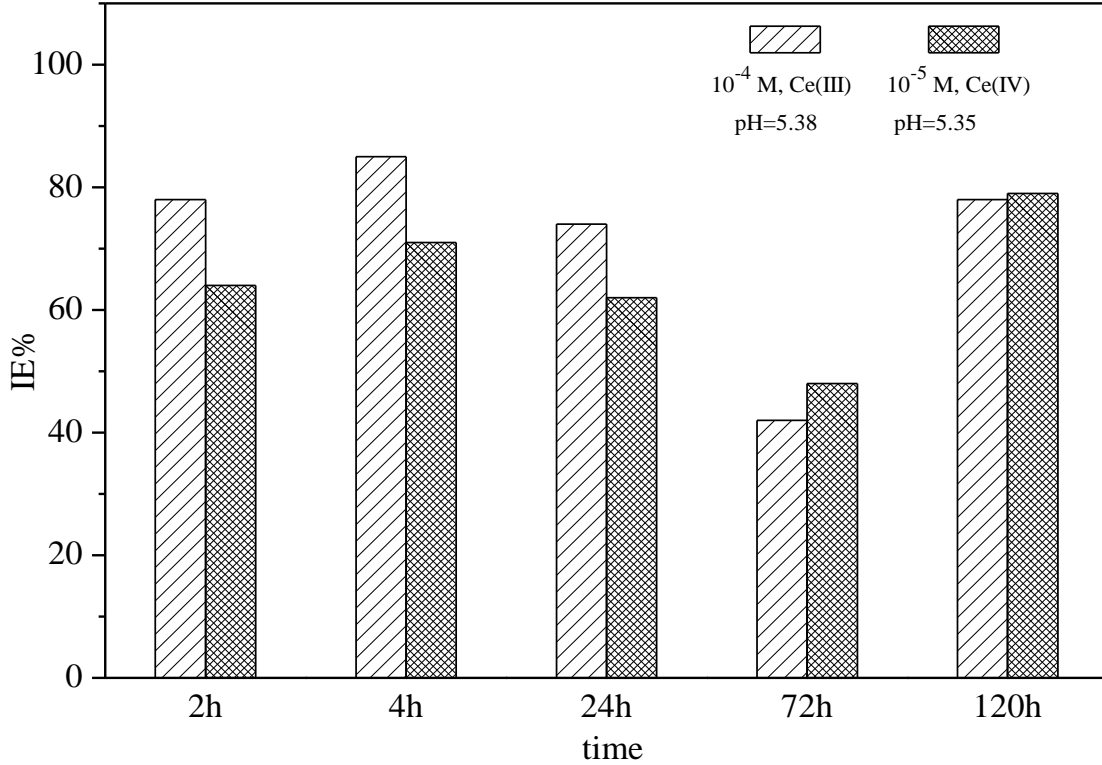


**Figure 33.** Values of the inhibitor's efficiency of Ce(III) and Ce(IV) ions after different times of exposure of the samples into 3.5 % NaCl solution.

Figure 33 illustrates the values of inhibition efficiency (IE %) and their evolution within the time of exposition of the samples into the corrosive medium. It is necessary to remark that the comparison was done for solutions with similar values of pH, but not at equal concentrations of the Ce(III) and Ce(IV) salts. This approach (for comparison) was executed, due to the fact that the solutions with equal concentrations of Ce(III) and Ce(IV) possess rather different pH values. Really, as it could be seen from Table 9, the solution of  $10^{-3}$  M Ce(III) ammonium nitrate, has pH = 4.20. At the same value of concentration, the Ce(IV) possess pH = 2.69, and in the latter case, the cerium ions act rather as activators of the aluminium alloy corrosion.

Evidently is from Figures 31, 32 and 33, that the inhibitive effect of Ce(III) ions excels that of Ce(IV) ions. It seems that at inhibition by Ce(III) ions, a mixture of

precipitates appears, composed by hydroxides of both ions and their composition enables achievement of higher inhibitive effect. Figure 33 shows also that the inhibitive efficiency increases, at the initial hours of exposure of the samples into the corrosive medium. Obviously, the formation of oxides/hydroxides of both ions and their precipitation are not immediate processes. However, after extended exposure time, decrease of the inhibitive efficiency is observable. Parkhill and co-authors [30] suggest that when the thickness of the inhibitor's precipitates reaches defined a critical value and delaminating of the inhibitor's precipitates begins. For the present case, this suggestion is not acceptable. The quick decrease of the inhibitive efficiency is consequence of the remarkable rate of dilution of the solution of both ions. After prolonged exposure, because of the simultaneous initiation and size growth of the corroded areas (pittings), inhibitor's expense occurred. Consequently, the quantity of the inhibitor is not enough to cover the newly formed corrosion sides.

The quick expense of the inhibitor, leads to corrosion acceleration, enhancing the formation of corrosion products. These products begin to hinder the corrosion process. The increase of the inhibitive effect after 120 hours of exposure in the corrosive medium is rather consequence of sedimentation of corrosion products, which causes retention the anodic reaction of alloy's dissolution.

#### **5.4. *Surface topology observations:***

Additive topographic observations were performed after the corrosion tests. They were applied in order to confirm the conclusions done after the analysis of the results of the electrochemical measurements. Figure 34 shows dark orange sediment, deposited after exposure of sample of AA2024 to solution of NaCl, with addition of cerium ammonium nitrate, which showed a high level of corrosion inhibition.

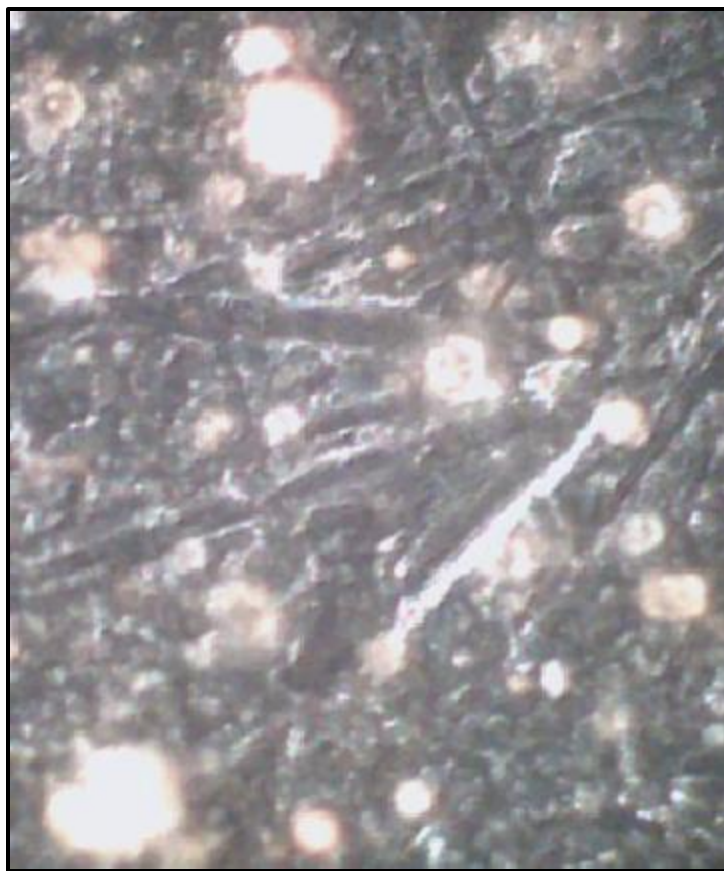


**Figure 34.** Optic micrograph of Ce-sediments on sample's surface

These orange nodules were formed on localised areas of the sample's surface. They were randomly spread on the entire surface subjected to the inhibitor containing corrosive medium. These observations confirm all of the conclusions done for the electrochemical measurements.

Further, observations by Scanning Electronic Microscopy were performed on the same sample. Figures 35 and 36 represent the superficial morphology of a sample, after exposure to inhibitor containing NaCl solution.

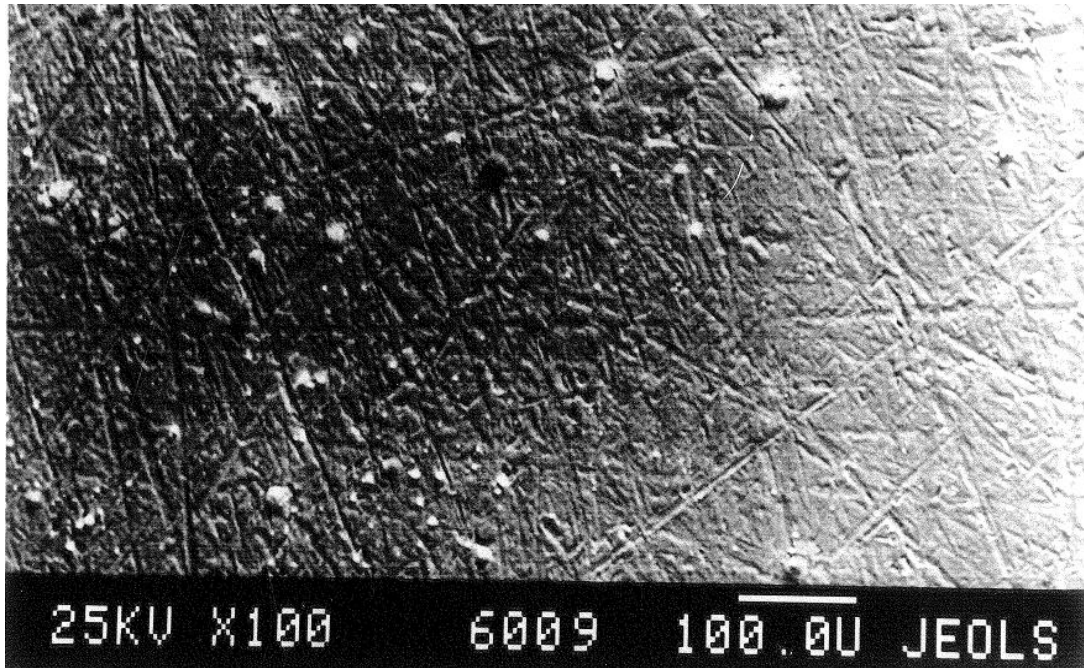


**Figure 35.** Image obtained by SEM - surface of AA2024 with nodules of inhibitor's sediments, magnification x100, resolution 100  $\mu\text{m}$

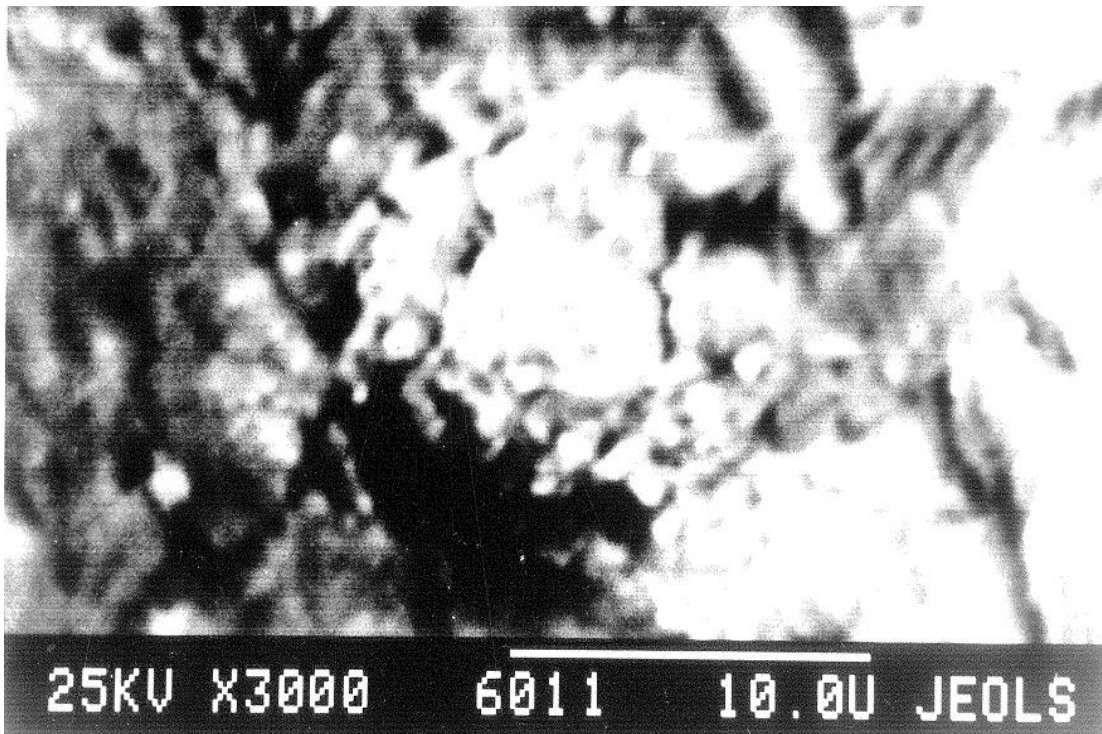


**Figure 36.** Image obtained by BSE - surface of AA2024 with nodules of inhibitor's sediments, magnification x3000, resolution 10  $\mu\text{m}$

The results of the analysis of the electrochemical measurements, and the posterior modeling by fitting to appropriated equivalent circuits, were confirmed by the observations performed by crystallographic optical, and scanning electronic microscopes.

Taking in account all of the concepts described in the present work, the following image could be drawn as adequate one.

- 1- The AA2024 alloy forms clearly expressed cathodic and anodic areas because of intermetallic alloying elements in its composition.
- 2- The Ce-ions represented in the corrosive medium form sediments which precipitate particularly on the cathodic sites.

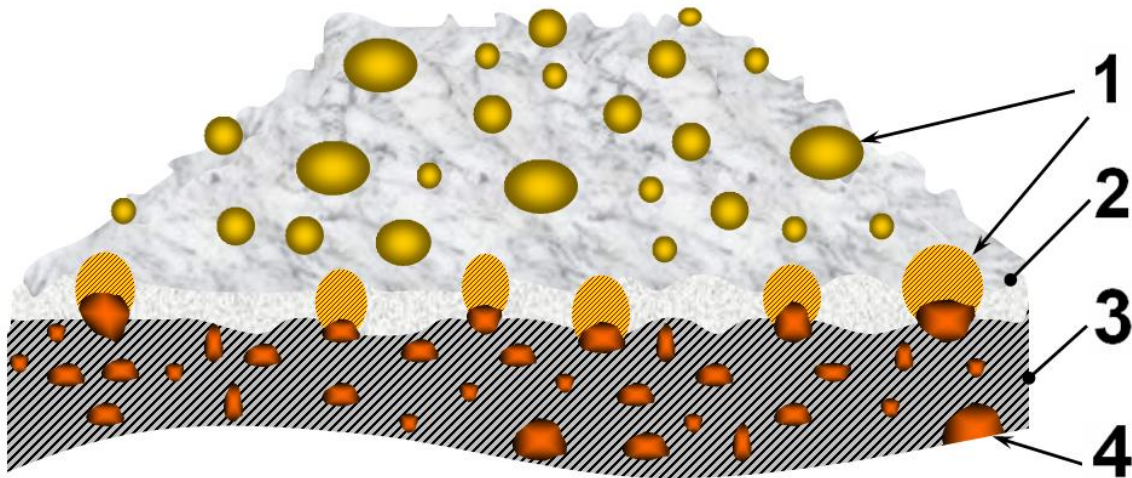


**Figure 37.** Visual model of Aluminium alloy with inhibitor deposits on its surface

1 – inhibitor deposits; 2 – surface oxide layer; 3- aluminium matrix; 4 – intermetallic inclusions

The investigations over the corrosion processes are related to detailed description of the chemical processes (oxidation, reduction), and the accompanying physical-chemical processes, adsorption, dissolution and etc, The nature of the processes and their kinetics is entirely predetermined by the presence of the respective chemical reactants, and their concentrations. The nature, morphology and the rate of the corrosion processes depend on of the composition of the metal alloy, the composition of the corrosive medium and especially its pH, as well as the environmental conditions: temperature, time of exposition, etc.

## VI. CONCLUSIONS:

### 6. Conclusions obtained from the present research

1. The inhibitive effect of the cerium ions during the corrosion of AA2024 aluminium alloy in 3.5 % NaCl solution, almost entirely depends on the oxidation state of the corresponding ions.
2. It was established that Ce(III) ions reveal higher inhibitor's efficiency than ions of Ce(IV), when the respective ions are introduced in form of ammonium nitrates, and at equal measurements conditions and relatively equal values of pH, but with different concentrations for Ce(III) and Ce(IV).
3. It is shown that at higher concentrations of the respective Ce(III) and Ce(IV) ions in the corrosive medium act rather as activators (promoters) of the corrosion. It was determined that the cerium ions possess a dualistic nature of interaction. Namely they act as inhibitors at lower concentrations, and activators at higher concentrations. It was established that this behavior is a result of the hydrolysis process going on of the respective cerium salts in aqueous media.
4. With extension of the exposure time of the samples in the corrosive medium up to 120 hours, an increasing of the inhibitive efficiency was observed. This increase is not a result of the Ce-ions, but rather it is consequence of sediments behavior represented as gradients in the corrosion products on the sample's surface.
5. The quantitative results for the inhibitor's efficiency of both of the cerium salts, obtained by the polarization measurements, were confirmed by the analyses of the acquired impedance spectra. By structural impedance modeling were obtained data for the parameters of the oxide layer, as well as the processes involved to the charge transfer  $R_{ct}$  through the metal / electrolyte interface. It is

shown that this measure ( $R_{ct}$ ), for the passive metals is a part of the polarization resistance  $R_p$ , which values were obtained by the polarization measurements.

6. It was discovered that when the currents are higher, that is more intensive corrosion, the  $E_{corr}$  are nobler, but this is not caused by inhibition effect, it could be explained by the high quantity of corrosion products produced by the corrosion reactions. They cover the anodic zones of the sample's surface, in form of sediments.
7. The surface observations performed by means of optical crystallographic microscopy (OCM) and scanning electronic microscopy (SEM) have undoubtedly evidenced that the precipitates of the Cerium inhibitor formed a globular dark orange bodies predominately deposited on local areas of the surface. In accordance with other scientific publications our suggestion is that these local areas are the cathodic ones.

## VII. REFERENCES

- [1] E.A. Starke and J. T. Staley: Progress Aerospace Science 32 (1996) 131.
- [2] AIRBUS A380, *Airplane characteristics*, Issue 30.03.05 (2005), [www.content.airbusworld.com/SITES/Technical.../AC\\_A380.pdf](http://www.content.airbusworld.com/SITES/Technical.../AC_A380.pdf)
- [3] K. A. Yasakau, M. L. Zheludkevich, S. V. Lamaka and M. G. S. Ferreira: *Mechanism of Corrosion Inhibition of AA2024 by Rare-Earth Compounds*, J. Phys. Chem. B, 110 (2006) pp. 5515 – 5528
- [4] P. Camperstini, H. Terryn, A. Hovestad and J. H. de Wit: Surf. Coating Tech. 176 (2004) 365
- [5] M. L. Zheludkevich, K. A. Yasakau, S. K. Poznya and M. G. S. Ferreira: Corros. Sci. 47 (2005) 3368.
- [6] I. T. E. Fonseca, N. Lima, J. A. Rodrigues, M. I. S. Pereira, J. C. S. Salvado and M. G. S. Ferreira: Electrochem. Commun. 4 (2002) 353.
- [7] P. Campestrini, E. P. M. van Westing, H. W. van Rooijen and J. H. de Wit: Corros. Sci. 42 (2000) 1853.
- [8] A. Boag, A.E. Hughes, A. M. Glenn, T. H. Muster, D. McCulloch: *Corrosion of AA2024-T3 Part I: Localised corrosion of isolated IM particles*. Corrosion science xxx, (2010), xxx IN PRESS.
- [9] A. E. Hughes, C. MacRae, N. Wilson, A. Torpy, T. H. Muster, A. M. Glenn, Surf. Int. Anal. 42 (9), (2010) 334 – 338
- [10] M. Kendig, S. Jeanjaquet, R. Addison, J. Waldrop, Role of hexavalent chromium in the inhibition of corrosion of aluminium alloys, Surf. Coat. Technol. 140 (2001) 58-66
- [11] Shem M., Schmidt T., Caparrotti H., Wittmar M., and M. Veith: *Corrosion inhibiting cerium compounds for chromium-free corrosion protective coatings on AA 2024*, Proceed, Eurocorr 2007, Freiburg, Germany (2007).
- [12] Zheludkevich M., Salvado I. and Ferreira M.: *Sol-gel coatings for corrosion protection of metals*, J. Materials Chemistry, 15 (2005) pp. 5099-5111.
- [13] Gusmano G. and Montesperelli G.: *Zirconia primers for corrosion resistant coatings*, Surface and Coatings Technology, 201 (2007) 5822-5828.

- [14] M. Zheludkevich, R. Serra, M. Montemor and M. Ferreira., *Oxide nanoparticle reservoirs for storage and prolonged release of the corrosion inhibitors*, *Electrochem. Commun.* **7** (2005) 836
- [15] S. Lamaka, M. Zheludkevich, K. Yasakau, R. Serra, S.K. Poznyak and M. Ferreira, *Progress in Organic Coatings* **58**, 2007, 127–135.
- [16] N. Voevodin, N. Grebush, W. Soto, F. Arnold and M. Donley: *Potentiodynamic evaluation of Sol-Gel Coatings with inorganic inhibitors*, *Surf. Coat. Tech.* **140** (2001) 24 – 28
- [17] A. S. Hamdy and A. M. Beccaria, *Effect of surface preparation prior to cerium pre-treatment on the corrosion protection performance of aluminum composites*, *J. Appl. Electrochem.* **35**, (2005), 473–478
- [18] A. Aldykiewicz, A. Davenport and H. Issacs, *J. Electrochem. Soc.* **143** (1996) 147 – 155
- [18] M. L. Zheludkevich R. Serra, M. F. Montemor, K. A. Yasakau I. M. Miranda Salvado, M. G. S. Ferreira: *Nanostructured sol-gel coatings doped with cerium nitrate as pre-treatments for AA2024-T3 Corrosion protection performance*. *Electrochimica Acta* **51** (2005) 208 - 217
- [19] P. Suegama, H. de Melo, A. Benedetti, I. Aoki: *Influence of cerium (IV) ions on the mechanism of organosilane polymerization and on the improvement of its barrier properties*. *Electrochimica Acta* **54** (2009) 2655–2662
- [20] S. Lamakaa, M. Zheludkevich, K. Yasakau, R. Serra, S. Poznyak and M. Ferreira: *Nanoporous titania interlayer as reservoir of corrosion inhibitors for coatings with self-healing ability* *Progress in Organic Coatings* **58** (2007) 127– 135
- [21] S. Tamborim, A. Maisonnave, D. Azambuja and G. Englert: *An electrochemical and superficial assessment of the corrosion behavior of AA 2024-T3 treated with metacryloxypropylmethoxysilane and cerium nitrate*. *Surface and Coatings Technology* **202** (2008) 5991–6001
- [22] S. Kozhukharov: *Relationship between the conditions of preparation by the sol-gel route and the properties of the obtained products*. *Jour. Univ. Chem. Tech. Met.* **44** (2), (2009) 143 – 150
- [23] Eloisa Cordoncillo Cordoncillo: *Preparación de vidrios basados en una matriz de sílice con procesado sol-gel, aplicación a la obtención de nuevos vidrios ópticos de cinc y cadmio*. Doctoral thesis Castellón (Spain) 1995, pp. 16.
- [24] P.E. López, J. B. Carda Castello, E. C. Cordoncillo: *Esmaltes y pigmentos Ceramicos*. Editor: Faenza Editrice Iberica (Castellón), 2001, pp. 255

- [25] K.Yasakau, M. Zheludkevich and O. Karavali: *Influence of inhibitor addition on the corrosion protection performance of sol – gel coatings on AA2024*. Progress in organic coatings 63 (2008) 352 – 361
- [26] G. Cicileo, B. Rosales, F. Varela, and J.Vilche, Corros. Sci. 40 (1998) 1915 – 1921
- [27] I. Devol and E. Bardez, J. Colloid Interface Sci. 200 (1998) 241 – 250
- [28] S. Lamaka, M. Zheludkevich, K.Yasakau, M. Montemor and M. Ferreira: *High effective organic corrosion inhibitors for 2024 aluminium alloy*. Electrochim Acta 52 (2007) 7231 – 7247
- [29] A. Onal and A. Aksut, Anti-Corr Met. Mat. 47 (2000) 339 - 344
- [30] R. Parkhill, E. Knobbe and M.Donley, Prog. Org. Coat. 41 (2001) 261 – 269
- [31] J. Davis, ASM International, *Corrosion: Understanding the Basics*” American Technical Publishers Ltd, Materials Park, Ohio, (2000) p. 10.
- [32] R. Petrucci, W. Harwood: *Química general. Principios y aplicaciones modernas* ISBN: 84-8322-043-1 editor Prentice Hall Iberia, S.L.R. 1998 p. 747
- [33] I. Nenov “Bases of electrochemistry” Gov. Ed. “Technicka” Sofia – 1989, p. 367
- [34] D.H. Lister, W.G. Cook: *UNI001: Reactor chemistry and corrosion*. Section 13: Kinetics of Aqueous Corrosion accessible via Internet
- [35] R. Petrucci, W. Harwood: *Química General. Principios y aplicaciones modernas* Prentice Hall Iberia S.R.L. Madrid 1999, pp. 730 – 732
- [36] F. Scholz: *Electroanalytical methods. Theory and practice*. Publ. house “Laboratory of knowledge” Moskow 2006, p.29
- [37] I. Nenov: *Bases of electrochemistry*. Gov. Ed. “Technicka” Sofia – 1989, p. 130
- [38] T. O’Keefe, P. Yu, S. Hayes, A. Williams, M. O’Keefe: *Fundamental Evaluation of the Deposition of Cerium Oxide*. Materials Research Center, University of Missouri-Rolla, accessible via Internet
- [39] J. Vogelsang: *The new standards for EIS measurements on coatings*. Short course on EIS proceeds. 6 – 7 (2008) Portugal
- [40] M. C. D’ocon Navaza, M. J. G. Garcia-Saavedra, J. C. V. Garcia: *Fundamentos y tecnicas de analisis bioquímico*. Publ. House Artes Graficas Cuesta – Madrid 1998; pp. 147 – 157

- [41] M. Bethencourt, F. J. Botana, M. Marcos, J. M. Sánchez-Amaya, L. González-Rovira: *Behaviour of the alloy AA2017 in aqueous solutions of NaCl. Part I: Corrosion mechanisms*. Corrosion Science 51 (2009) 518-524.
- [42] E. M. Sherif and Su-Moon Park; Journal of The Electrochemical Society, 152 (6) (2005) 205-211
- [43] E. M. Sherif and Su-Moon Park; Electrochimica Acta 51 (2006) 1313-1321
- [44] M. L. Zheludkevich, M.F. Montemor, I. M. Miranda Salvado, M.G.S. Ferreira; Electrochimistry communications 7 (2005) 836 - 840
- [45] M. L. Zheludkevich, R. Serra, M.F. Montemor, K. A. Yasakau, I. M. Miranda Salvado, M.G.S. Ferreira; Electrochimica Acta 51 (2) (2005) 208 - 217
- [46] *User manual for AUTOLAB Instruments*-Appendix IX, "Fra for Windows 4.9"; edition of Ecochemie (Netherlands) year 2004, page 88
- [47] B. A. Boukamp, J. Electrochem. Soc. 142, (1995) 1885
- [48] S. Vlahov, A. Ivanov: *General Microbiology*, Kl. Okhridsky ed. Sofia (1996) p. 12
- [49] Purificación Escribano López, Juan B. Carda Castelló, Eloísa Cordoncillo Cordoncillo: *Esmaltes y pigmentos cerámicos*. Faenza Editrice Ibérica S.L. ; Castellón (2001) pp. 279-288.
- [50] J. S. Fritz, G. H. Schenk, Quant. Analyt. Chem. Ed. House "Mir" – 1978 – Moscow. p. 222.
- [51] A. J. Aldikewicz, H. S. Isaacs, A. J. Davenport, Electrochem. Soc. 142 (1995) 3342.
- [52] A. J. Aldikewicz, H. S. Isaacs, A. J. Davenport, Electrochem. Soc. 143 (1996) 147.
- [53] A. J. Davenport, H. S. Isaacs, M. W. Kendig, Corros. Sci. 32 (1991) 653.
- [54] M. Bethencourt, F. J. Botana, M. J. Cano, M. Marcos, J. M. Sanchez - Amaya, L. Gonzalez - Rovira, Corros. Sci. 51 (2009) 518.
- [55] K. Aramaki, Corros. Sci. 43 (2001) 1573.
- [56] C. Jeyabrabha, S. Sathiyarayanan, G. Venkatachari: *Effect of cerium ions on corrosion inhibition of PANI for iron in 0.5 M H<sub>2</sub>SO<sub>4</sub>*. Applied Surface Science 253 (2006) 432 – 438

- [57] K. F. Khaled, M. M. Al-Qahtani: *The inhibitive effect of some tetrazole derivatives towards Al corrosion in acid solution: Chemical, electrochemical and theoretical studies*. Materials Chemistry and Physics 113 (2009) 150 – 158
- [58] R. Rosliza, W. B. Wan Nik: *The effect of inhibitor on the corrosion of aluminum alloys in acidic solutions*. Materials Chemistry and physics 107 (2008) 281 – 288
- [59] Ajit Kumar Mishra, R. Balasubramaniam: *Corrosion inhibition of aluminium by rare Earth chlorides*. Materials Chemistry & Physics 103 (2007) 385 – 393
- [60] Ajit Kumar Mishra, R. Balasubramaniam: *Corrosion inhibition of aluminium alloy AA2014 by rare earth chlorides*. Corrosion Science 49 (2007) 1027 – 1044